Fábio Alexandre Mouzinho de Sousa Pinto

Development of a Bi-layer Hydrogel via 3D Printing for Articular Cartilage Replacement: PVA/Chitosan/HAp/CNF Scaffold with a PVA/Tannic Acid Surface

Master's Thesis Report in **Biomedical Engineering**

ADVISER

Professor Doutor Célio Gabriel Figueiredo Pina

Professora Doutora Carla Maria de Almeida Amorim Carneiro

December of 2025

PRR Plano de Recuperação e Resiliência
REPÚBLICA PORTUGUESA
Financiado pela União Europeia NextGenerationEU

Fábio Alexandre Mouzinho de Sousa Pinto

Development of a Bi-layer Hydrogel via 3D Printing for Articular Cartilage Replacement: PVA/Chitosan/HAp/CNF Scaffold with a PVA/Tannic Acid Surface

Examination Committee

President:
Prof. Doutora Helena M. Caria
Polytechnic Institute of Setúbal
Advisers:
Prof. Doutor Célio G. Pina
Polytechnic Institute of Setúbal

Member:
Prof. Doutora Ana Paula V. A. do Serro
University of Lisbon at Instituto Superior Técnico

December of 2025

Acknowledgements

The completion of this dissertation represents the culmination of an academic, scientific, and personal journey that was only made possible through the contribution, support, and dedication of several institutions and individuals, to whom I express my deepest gratitude.

First and foremost, I would like to thank the Polytechnic Institute of Setúbal, the Instituto Superior Técnico, the Egas Moniz School of Health & Science, and the Nuclear Technology Centre of Instituto Superior Técnico for their hospitality and for providing access to the essential resources needed for the development of this work.

I extend special thanks to my supervisors, Professor Célio Gabriel Figueiredo Pina and Professor Carla Maria de Almeida Amorim Carneiro, for their guidance, constant availability, encouragement, and the trust they placed in me.

I am also grateful to Professor Ana Paula Serro of Instituto Superior Técnico, Professor Madalena Salema Oom of the Egas Moniz School of Health & Science, and Engineer Paula Matos of the Nuclear Technology Centre, for all their technical and scientific support, for sharing their knowledge, for their practical guidance, and for the generosity with which they always welcomed and accompanied me.

My heartfelt thanks go to my family, who always believed in me and gave me the strength to continue at every moment. To my girlfriend, for her affection, patience, and constant encouragement, even during the most demanding periods of this journey. And to my friends, for their understanding, motivation, and companionship, which made this path lighter.

To all of you, my sincere gratitude. Without your contribution, this work would not have been possible.

Abstract

This investigation develops and characterizes a bi-layer hydrogel system designed for articular cartilage regeneration, combining a robocasted PVA scaffold reinforced with hydroxyapatite, chitosan, and cellulose nanofibers, with an upper PVA/tannic acid layer engineered to optimize lubrication and bioadhesion. The paste formulation enabled a pseudoplastic rheological behaviour suitable for 3D printing, resulting in mechanically stable porous structures with controlled geometry. The upper layer exhibited homogeneous surfaces, a low coefficient of friction, and effective integration with the scaffold, forming a continuous hybrid construct. Mechanical, tribological, chemical, and swelling analyses demonstrated that the bi-layer architecture simultaneously enhances strength, stability, and lubricating performance. Biological studies confirmed high cell viability and adequate adhesion in the irradiated versions. Overall, the results validate the potential of this system as a promising platform for cartilage replacement and regeneration, highlighting the role of polymeric combinations and additive manufacturing in tissue engineering.

Keywords: Bi-layer hydrogel, articular cartilage regeneration, robocasting, PVA-based composites, tannic acid lubrication, additive manufacturing

Resumo

Esta investigação pretende desenvolver e caracterizar um sistema hidrogel bicamada destinado à regeneração da cartilagem articular, que combina um scaffold produzido por robocasting de PVA reforçado com hidroxiapatite, quitosano e nanofibras de celulose, e uma camada superior de PVA/ácido tânico concebida para otimizar a lubrificação e a bioadesão. A formulação das pastas permitiu obter um comportamento reológico pseudoplástico adequado à impressão 3D, resultando em estruturas porosas mecanicamente estáveis e com geometria controlada. A camada superior revelou superfícies homogéneas, baixo coeficiente de fricção e integração eficaz com o scaffold, formando um scaffold híbrido contínuo. Ensaios mecânicos, tribológicos, químicos e de intumescimento demonstraram que a arquitetura bicamada melhora simultaneamente a resistência, estabilidade e desempenho lubrificante. Estudos biológicos confirmaram elevada viabilidade celular e adesão adequada nas versões irradiadas. Os resultados validam o potencial deste sistema como plataforma promissora para substituição e regeneração de cartilagem, destacando o papel das combinações poliméricas e da manufatura aditiva na engenharia de tecidos.

Palavras-chave: Hidrogel bi-camada, regeneração de cartilagem articular, robocasting, compósitos à base de PVA, lubrificação com ácido tânico, manufatura aditiva

Contents

List of Figures

List of Tables

Acronyms

AC	Articular Cartilage
ACI	Autologous Chondrocyte Implantation
AM	Additive Manufacturing
AMIC	Autologous Matrix-Induced Chondrogenesis
CAD	Computer Assisted Design
CNFs	Cellulose Nanofibers
CO2	Carbon Dioxide
CoF	Coefficient of Friction
CTN	Chitosan
DIW	Direct Ink Writing
EDS	Energy-dispersive X-ray Spectroscopy
EMEM	Eagle´s Minimum Essential Medium
EWC	Equilibrium Water Content
FBS	Fetal Bovine Serum
FTIR	Fourier-transform Infrared
HAp	Hydroxyapatite
HCL	Hydrochloric Acid
IPNs	Interpenetrating Networks
MACI	Matrix-Assisted Chondrocyte Implantation
OA	Osteoarthritis
PBS	Phosphate-Buffered Saline
PVA	Poly(vinyl alcohol)
RA	Rheumatoid Arthritis
RT	Room Temperature
SEM	Scanning Electron Microscope
SWC	Swelling Capacity
TA	Tannic Acid
TKA	Total Knee Arthroplasty
WHO	World Health Organization
3D	Three dimensional

List of Symbols

W_d	Weight of the dried sample
W_h	Weight of the hydrated sample
E_T	Tangent Compressive Modulus
ε	Strain
$\Delta\varepsilon$	Strain variation
σ	Stress
μ	CoF
F_T	Frictional force
F_N	Normal load
F	Force
A	Area
P	Pressure

1. Introduction

Articular cartilage plays a fundamental role in joint biomechanics, enabling smooth and frictionless movement, uniformly distributing mechanical loads, and protecting the subchondral bone. Its specialized structure, composed of a dense extracellular matrix, low cellularly, and a zonally organized structure, grants it exceptional mechanical behaviour, particularly in terms of shock absorption and lubrification properties but also severely limits its ability to self-repair. Because it is avascular, aneural, and lacks progenitor cells, even small lesions fail to heal and can progress to inflammation, pain, reduced mobility, and degenerative changes such as osteoarthritis. As life expectancy increases, this condition has become one of the most common musculoskeletal disorders, with significant clinical and socioeconomic impact.

Despite extensive research, no current clinical intervention is capable of fully restoring the structure and function of native articular cartilage. Existing therapeutic options, from palliative care to reparative and reconstructive procedures, often represent significant drawbacks, including limited durability, variable outcomes, surgical complexity, donor-site morbidity, and graft-related risks. This underscores the need for new regenerative strategies capable of providing both the mechanical resilience and biological functionality required for long-term cartilage restoration.

Recent advances in biomaterials, hydrogels, additive manufacturing, and composite scaffolds offer new strategies for cartilage repair. Hydrogels are particularly promising due to their biocompatibility, tuneable mechanics, and ability to mimic native cartilage. However, challenges remain, including limited compressive strength, structural instability, swelling, degradation, and poor adhesion to cartilage and bone surfaces.

Additive manufacturing techniques, particularly material extrusion and robocasting, enable the fabrication of customized scaffolds with controlled porosity, geometry, and mechanical properties. Robocasting deposits viscous polymeric pastes layer-by-layer with high precision, producing structures that provide mechanical support and promote cell infiltration. Additionally, the ability to tailor these scaffolds to patient specific anatomies makes them suitable for repairing irregular cartilage defects.

The present investigation addresses the clinical and technological limitations of current cartilage repair approaches by developing and characterizing a robocasted PVA-

based composite hydrogel system. Building advances such as the reinforcement of PVA with HAp, chitosan and nanocellulose, and the use of tannic acid to enhance surface performance, this work proposes a bi-layer implant that combines the strength of a structural scaffold with the lubricity of a functional hydrogel coating. The lower layer is a mechanically robust, porous scaffold produced via robocasting, designed to support cell attachment and improve anchorage to subchondral bone, while the upper layer is a cast-dried PVA/tannic acid hydrogel that provides smoothness, lubrication and adhesion.

Together, these components form a hybrid construct that better mimics the functional and mechanical properties of native cartilage than single-material implants. Through a comprehensive evaluation of its rheological, mechanical, morphological, tribological and biological behaviour, this study aims to validate the feasibility of the proposed system and to clarify how multi-component hydrogels can overcome key limitations of current substitutes.

1.1. Motivation

This investigation arises from the unmet clinical need for robust, durable, and biologically compatible solutions for articular cartilage defects. Current treatments, including microfracture, autologous chondrocyte implantation, mosaicplasty, and allografts, present limitations such as donor site morbidity, poor long-term outcomes, surgical complexity, or risk of immune rejection. Substitution approaches like total joint arthroplasty, while effective in advanced degeneration, are invasive and unsuitable for younger patients.

Hydrogels have emerged as promising alternative due to their similarity to native cartilage and their ability to provide lubrication, support cellular activity, and be tailored to specific biophysical requirements. However, challenges such as insufficient mechanical strength, difficulty in ensuring firm adhesion to surrounding tissues, and variable biocompatibility remain unresolved.

Technological advances, particularly in 3D printing/robocasting, biomechanical characterization and composite hydrogel formulation, motivate the development of new implantable constructs. Additionally, the integration of components such as PVA,

chitosan, hydroxyapatite, cellulose nanofibers, and tannic acid allow fine-tuning properties like stiffness, friction, water retention, and bioadhesion.

The benefits expected from this study include improved integration with subchondral bone, enhanced lubrication at the cartilage-cartilage interface, and an approach that can be customized to patient-specific geometries through additive manufacturing. These advances have the potential to support performance, creating scaffolds that better support long-term regeneration.

1.2. Objectives

The main objective of this dissertation is to develop and characterize a bi-layer hydrogel-scaffold composite suitable for articular cartilage regeneration. To achieve this goal, the following specific objectives were defined:

- Formulate a printable polymeric paste using PVA and reinforcing components (HAp, chitosan, cellulose nanofibers) optimized for robocasting.
- Fabricate mechanically stable scaffolds with a well-defined internal geometry designed to promote cell infiltration and mechanical resistance.
- Produce upper hydrogel layers based on PVA/tannic acid mixtures with tunable stiffness, frictional properties, and bioadhesion.
- Integrate both layers into a single bi-layer construct through controlled drying and adhesion mechanisms.
- Characterize the materials' rheology, morphology (macro and microscale), chemical structure, swelling behaviour, mechanical performance, tribological behaviour, and biological response.
- Evaluate and compare irradiated versus non-irradiated samples to determine effects on crosslinking, degradation, and cytotoxicity.
- Identify the limitations and potential of the constructed system for future developments in cartilage replacement technologies.

These objectives guide the investigation toward understanding how composition, fabrication method, and multi-layer integration influence the functional performance of the final implant.

1.3. Structure

This dissertation is organized into 6 chapters with corresponding sub-chapters, a references section, and 1 appendix. A brief overview of each chapter is presented below.

- Chapter 1 – Introduction: presents the clinical motivation, objectives and proposed solution for this investigation.
- Chapter 2 – Literature review: this chapter reviews the current knowledge on articular cartilage, its structure, mechanical and tribological properties, common pathologies, and existing treatment strategies. It also discusses hydrogels, their classification, composite formulations, and additive manufacturing approaches, highlighting the challenges and opportunities for cartilage tissue engineering.
- Chapter 3 – Methods and materials: describes in detail the preparation, fabrication, and characterization methods applied to scaffolds, hydrogels, and bi-layer constructs.
- Chapter 4 – Results: presents the experimental results obtained throughout this investigation.
- Chapter 5 – Discussion: interprets the results, analyses fabrication challenges, and compares findings with existing literature.
- Chapter 6 – Conclusion: summarizes the main outcomes and suggests improvements and future research directions.

2. Literature Review

This chapter provides an overview of current knowledge on cartilage structure, function, and pathologies, with a focus on articular cartilage due to its complex biomechanics and clinical relevance. It also discusses treatment strategies, from palliative approaches to tissue engineering solutions, highlighting hydrogels (particularly PVA-based composites) and their potential in cartilage repair. Finally, the chapter introduces additive manufacturing, especially robocasting, as a tool for creating customized scaffolds that support tissue regeneration and mimic native cartilage properties.

2.1. Cartilage

Human cartilage is a specialized connective tissue with several different functions that contribute to the support and protection of certain structures in the human body. This conglomerate of tissues, surrounded by a fibrous membrane called the perichondrium, is composed by chondrocytes, the primary cells of this material, in association with several other components such as proteoglycans, glycosaminoglycans and collagen, which are responsible for forming the cartilage matrix itself [1]. However, this type of material is notorious for two main reasons. It lacks any kind of irrigation or nervous connections. The absence of irrigation is one of the main reasons why it is so difficult to regenerate, being that the only way it can get its nutrients and eliminate waste is by diffusion with the surrounding tissues. Additionally, the absence of nervous connections in cartilage renders no physical sensation to indicate damage, which can delay the detection of injuries [1]. Nonetheless, regardless of its limitations, cartilage should not be thought of as a single material, as there are several types of cartilage that differ in their inherent structure and relevant function [1].

Hyaline cartilage is the most abundant type of cartilage in the human body. It consists mainly of collagen and proteoglycans. As the most common type, this cartilage can be found in various familiar places such as the nose, trachea, sternum and a handful of segments on the ribs. The main characteristic of this type of cartilage is its ability to withstand compressive forces and its extreme resistance to wear [1, 2].

Another type of cartilage is the elastic cartilage, which is the softest and most flexible of the other types. Its composition is like that of hyaline cartilage, but it has a component that is not present or detectable in hyaline cartilage, namely elastin fibres, which could

explain its flexibility. It is because of this property, which allows this type of cartilage to resist pressure, that elastic cartilage is commonly found in the larynx, epiglottis, ears and eustachian tube [1, 3].

Finally, the last type of cartilage is fibrocartilage. This cartilage is very capable of withstanding high levels of tension and compression. Its composition varies dynamically, either in terms of the materials it is made up of or the way it reacts to external factors such as mechanical stress. Because of its resistance to stress, this type of cartilage is often found in tendons, ligaments, discs and menisci [1, 4].

Among the types of cartilage described, articular cartilage, a specialised subtype of hyaline cartilage, is of particular interest because of its remarkable ability to withstand compressive forces and facilitate almost frictionless joint articulation. This tissue, essential for the proper functioning of synovial joints, is a key focus in research addressing joint degeneration and tissue regeneration and due to its intricate structure, functionality, and the inherent limitations.

2.1.1. Articular Cartilage

As previously stated, the Articular Cartilage (AC) is categorised as part of a distinct type of cartilage, namely Hyaline Cartilage. This cartilage is of particular importance due to its role as a load-bearing structure that overlies the interaction between the surfaces of bone and cartilage in diarthrodial joints. In this capacity, it ensures a low-friction environment and the distribution of all the different loads to which the body is subjected [5, 6]. In resemblance to the other types of cartilage, the AC can be regarded as a composite material because of all the materials that were previously identified, which can be consulted in **Table 1**.

Table 1 – Various distinct materials that comprise the Articular Cartilage, in weight percentage [5].

Chondrocytes	1-10%
Water	70-80%
Collagen	12-14%
-Type II	10-12%
-Type IX	~1%
-Type XI	~1%
Proteoglycans	7-9%

-Hyaluronic Acid	6-8%
-Other proteoglycans	~1%
Mineral Materials	<4%
Matrix Proteins	<1%

Despite its reduced flexibility relative to elastic cartilage, the AC retains a degree of flexibility that enables deformation and subsequent return to its original shape. Some research even refers the AC as being a viscoelastic material [5]. Another aspect of the AC that increases its intricacy is the fact that this structure possesses zonal arrangements, where each zone has its own different biological and mechanical properties [5, 6]. These arrangements are subdivided into four zones, or layers, as illustrated in **Figure 1**.

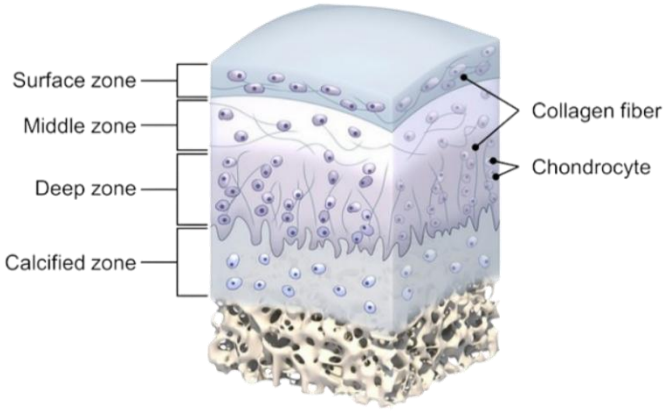

Figure 1 - Structure of the articular cartilage divided by its zones[6].

The first layer, also known as the superficial layer of the articular cartilage, makes up approximately 10–20% of the total AC thickness [5, 7]. This layer plays a critical role in protecting the deeper layers from shear stress and significantly influences the overall mechanical behaviour of the cartilage under load [5, 7]. The high-water content and low proteoglycan concentration of this layer contribute to its enhanced deformability in comparison to the more rigid inner zones of the cartilage. Any disruption to this layer increases the tissue's permeability, allowing for significant fluid exchange [5, 7].

The second layer of cartilage, or the middle layer, is the thickest, accounting for approximately 40–60% of the total cartilage thickness [5, 7]. It is characterised by a high concentration of proteoglycans and collagen fibrils, which play a crucial role in resisting compressive forces. This layer is also notable for its presence of chondrocytes, which are characterised by a spherical morphology and relatively low cell density [5, 7].

The third layer of cartilage, also known as the deep layer, comprises roughly 30% of the total cartilage thickness [5, 7]. It contains the largest collagen fibrils, the highest concentration of proteoglycans, and the lowest water content compared to the other layers. This layer also has a significant number of chondrocytes. The arrangement of collagen fibrils perpendicular to the articular surface makes this layer highly resistant to compressive forces [5, 7].

Finally, the fourth layer, otherwise known as the calcified layer, serves a vital role in anchoring the cartilage to the bone [5]. This layer has a low cellular density, with chondrocytes in a hypertrophic state. Its specialized composition provides high resistance to shear forces, reducing the likelihood of cartilage detachment from the bone.

From a general standpoint, the key takeaways from this are that there is a gradient in water and proteoglycan content. The concentration of water molecules tends to decrease with depth, while proteoglycan concentration increases. This is indicative of the functional and mechanical requirements of each layer. Despite the presence of collagen being almost invariable, its influence is represented not in quantity, but in the arrangement and size of its fibrils within each layer.

2.1.2. Tribomechanical properties of Articular Cartilage

In the context of the preceding remarks, it is of extreme importance to comprehend the mechanical and tribological properties of the cartilage, with a particular emphasis on the articular cartilage. These concepts are the key to understand how the cartilage behaves during its normal activity. It is important to refer that from a mechanical standpoint, the AC is a very complex material. For instance, it is anisotropic, which means that its behaviour varies depending on the direction of the load [7, 8]. Like it was mentioned before, the variation of its deformation under various stress-rates points to its viscoelasticity [7]. Even the layered structure of the cartilage influences in the way that the mechanical functions are performed through the thickness of the cartilage [7], which emphasises its heterogeneity and is directly connected to the composition of each layer and their role in the system. Due to its complexity, it is extremely difficult to acquire any kind of precise measurements *in vivo*, so most of the mechanical tests that are used to evaluate the AC's behaviour are done *in vitro*. These tests use different techniques, methods and devices to obtain the pertinent results regarding each property. Present in the following **Table 2** are the tribomechanical properties of native human articular cartilage.

Table 2 - Tribomechanical properties of native human articular cartilage [9, 10, 11, 12, 13].

	Value	Donor
Compressive Young's Module (MPa)	2-10	Human
Equilibrium Compressive Module (MPa)	0.79	Human
Poisson ratio	0.06 - 0,3	Human
Dynamic Shear Modulus (MPa)	0.1-4	Bovine
Equilibrious Shear Modulus (MPa)	0.05-0.25	Human
CoF (μ)	0.013-0.019	Human

As illustrated, numerous factors can influence the measured values in any given property. Due to the inherent complexity of articular cartilage, obtaining an absolute value for a specific property is challenging. Several variables contribute to this diversity, including:

- **Anatomical Region:** The site from where the sample was taken highly impacts the results, as different joint regions experience distinct loading conditions and require different mechanical demands [14, 15].
- **Donor Species:** While the AC of large mammals closely resembles that of a human in its properties, interspecies variations in composition and structural organization can lead to measurable differences [14, 15].
- **Depth-Dependent Characteristics:** The biomechanical properties of articular cartilage vary with depth due to the unique composition and organization of each histological zone [14, 15].
- **Loading Conditions:** Whether under dynamic or static loading, test results are influenced by the nature of the mechanical testing, particularly in relation to the viscoelastic behaviour of the articular cartilage [14, 15].

2.1.3. Articular cartilage's behaviour under compressive loading

As previously mentioned, the loading conditions of AC are a critical factor influencing its mechanical response under compression. AC exhibits a poro-viscoelastic behaviour, meaning that under rapid loading, the interstitial fluid retained within the matrix becomes pressurized and supports the majority of applied load. During sustained compression, fluid gradually exudes from the matrix, transferring a greater portion of the load to the solid matrix itself [16]. From a tribological perspective, AC maintains low friction under compression. Static loading reduces fluid support and increases friction due to fluid exudation and increased surface contact. In contrast, compressive loading combined with sliding motion can restore lubrication through tribological rehydration, where fluid is drawn back into the contact zone to re-establish a pressurized layer, reducing shear stress and friction. The decrease in friction is further enhanced by the increased stiffness of the tissue due to internal fluid pressure, which limits surface deformation [17, 18].

Assuming a healthy cartilage, these factors collectively determine the AC's behaviour under load. However, pathological conditions can compromise the tissue, in some cases leading to complete deterioration, which significantly alters its mechanical and tribological properties.

2.2. Pathologies affecting the Articular Cartilage

Due to its unique physiological structure, articular cartilage faces significant challenges in terms of nutrition and blood supply. This inherent limitation not only hinder its ability to self-repair but also reduce its capacity to absorb and utilize essential substances that could aid in the healing process of any damage inflicted to the AC. Such damage is often associated with sports or occupational activities, or from pathological conditions that specifically affect the joints.

One of the most diagnosed articular pathologies currently is Osteoarthritis (OA), which is a degenerative joint disease that affects multiple structures, which include articular cartilage, bone and synovial tissue. It is characterized by cartilage degradation, bone remodelling, and osteophyte formation. This can lead to pain, joint stiffness, swelling and reduced joint function [19]. According to the World Health Organization (WHO), approximately 528 million people were diagnosed with osteoarthritis in 2019, reflecting a 113% increase in its prevalence since 1990 [20]. The WHO also highlights

that osteoarthritis disproportionately affects certain social groups, with the highest prevalence observed among women and adults over the age of 55 [20].

Rheumatoid arthritis (RA) is a pathology like osteoarthritis but differs in being a systemic autoimmune disorder. It varies in severity and is commonly characterized by a chronic inflammatory process that damages not only the joints but also vital organs such as the heart, kidneys, and lungs. RA follows a fluctuating course with episodic exacerbations, and without proper treatment, it can lead to irreversible cartilage damage and significant impairment of joint function [21]. According to a WHO estimate, approximately 18 million people worldwide were living with RA in 2019. Like osteoarthritis, RA predominantly affects women and adults over the age of 55 [22].

Another prevalent concern is cartilage trauma, and its effects the tissue's tribomechanical properties. Experimental evidence demonstrates that a single traumatic impact can immediately alter the mechanical properties of articular cartilage, affecting both its stiffness and viscoelastic behaviour [23]. Epidemiological studies indicate that over than 40% of patients who experience any form of cartilage trauma are more susceptible to develop osteoarthritis later in life [24].

These pathologies represent a subset of diseases that specifically impact joint health and functionality. To mitigate their effects, a range of treatment strategies is utilized, from traditional approaches to the most advanced, innovative therapies.

2.3. Rheumatic Pathology Treatment Strategies

Despite being a prevalent issue in society, rheumatic pathologies have prompted the development of various medical strategies aimed at mitigating their effects or even restoring the functionality of affected joints and tissues. These strategies can be categorized based on their direct impact on treatment and therapeutic goals.

The primary treatment approaches can be classified into four distinct groups [25, 26]:

- **Palliation** – Techniques designed to alleviated symptoms and improve patient comfort without directly addressing the underlying cartilage damage.
- **Repair**: Techniques focused on directly repairing defects within the cartilage.

- **Restoration**: Techniques that stimulate the body's natural capacity for cartilage regeneration.
- **Substitution**: Techniques that replace damaged tissue to varying degrees, depending on the severity of the condition.

2.3.1. Palliation Techniques

Not all joint damage is severe or caused by chronic pathology, making it essential to offer treatments that addressed patient discomfort without invasive intervention. These palliative treatments aim to improve quality of life while delaying the progression of joint degeneration. Non-invasive approaches such as physical therapy, weight loss, and the use of braces or orthoses help improve joint function and alleviate pain. In more severe cases, steroid or hyaluronic acid injections are commonly applied to reduce inflammation and enhance joint lubrication [25, 26].

2.3.2. Repair Techniques

For localized cartilage defects, repair techniques are used to stimulate the tissue's natural healing response and restore structural integrity. Microfracture remains the most widely used method, involving small perforations in the damaged cartilage to access the subchondral bone, allowing bone marrow elements to form a fibrocartilaginous repair clot. Despite being widely used, these procedures do elevate some concerns about damaging the surrounding healthy tissues [25, 26, 27]. Other notable techniques are Nanofracture, which is like Microfacture, however uses smaller and deeper holes in a denser arrangement to reduce unwanted damage to surrounding tissues and allow for a more efficient treatment [28]. Finally, Autologous Matrix-Induced Chondrogenesis (AMIC) enhances this process by adding a collagen scaffold, which stabilizes the repair clot and supports more effective tissue regeneration, yielding better long-term outcomes [29].

2.3.3. Restoration Techniques

When repairing the damaged cartilage isn't sufficient, restoration techniques aim to re-establish cartilage tissue using cultured cells. Matrix-Assisted Chondrocyte Implantation (MACI) involves harvesting chondrocytes from healthy cartilage, culturing

them, and seeding them onto a biocompatible matrix before implantation into defect. Compared to traditional Autologous Chondrocyte Implantation (ACI), MACI reduces surgical complexity and periosteal-related complications while effectively regenerating cartilage [25, 26].

2.3.4. Substitution Techniques

Substitution techniques represent the final line of treatment for cartilage defects, typically reserved for cases where autologous cartilage degradation is too severe to be repaired or restored. Osteochondral Autograft Transfer (OAT) mosaicplasty transplants cylindrical cartilage-bone plugs from non-weight-bearing areas to the defect site, suitable for small lesions but limited by potential graft mismatch [30]. Osteochondral Allograft resolves the problem with the usage of non-weight-bearing tissue, although the risk of immune rejection from the recipient is a considerable risk. In cases of advance cartilage degeneration, examples like a Total Knee Arthroplasty (TKA) can be employed, where the natural cartilage is completely replaced with an artificial implant, though it requires an invasive procedure and extended rehabilitation [25].

2.3.5. Future Developments

The tissue regeneration field of medicine is always evolving. Current Techniques that are being developed aim to resolve most of the existing problems with the current available treatments by being easier to employ, cheaper or simply more effective. Some of these techniques are the application of growth factors that can regulate de differentiation and proliferation of cartilage regeneration process. A similar approach is the use of gene therapy, which aims to deliver genetic material capable of altering cell synthesis and function. Despite being very promising examples of treatments, neither of them has being tested in human trials [25].

A simpler and increasingly promising approach for treating cartilage defects is the use of hydrogels. These materials offer excellent lubrication and favourable mechanical properties, creating a flexible and durable matrix that supports cell proliferation and tissue regeneration. One of the key advantages of hydrogels is their tunability. Nearly all their defining characteristics – material composition, structural architecture, crosslinking density and resulting mechanical properties – can be precisely controlled to complement

each specific situation. These parameters play a critical role in regulating cellular behaviour and is ultimately responsible for influencing the fate of cells integrated within it [31].

Hydrogels represent a highly promising avenue in tissue engineering, largely due to their versatile fabrication methods, tuneable properties, and broad range of potential biomedical applications. Their adaptability makes them especially valuable for developing targeted, functional solutions in regenerative medicine.

2.4. Hydrogels

By definition, a hydrogel is a three-dimensional mesh of crosslinked polymers, which creates a singular, porous structure with the ability to absorb and store water, while maintaining its network structure. The hydrogel's ability to absorb water is essentially its swelling capacity, which depends on the hydrogel's hydrophilicity, the strength of the bond created by the crosslinking processes and the swelling media [32].

As mentioned before, this type of material is highly attractive for biomedical applications, which in part is due to its distinctive characteristic properties, such as biodegradability, biocompatibility, viscoelasticity, low friction and the ability to respond to different stimuli [32]. There are many ways of classifying a hydrogel as seen in **Figure 2**, but the most common criteria include the origin of polymer that is used, the type of cross-linking technique applied, the method of preparation and its charge [32, 33].

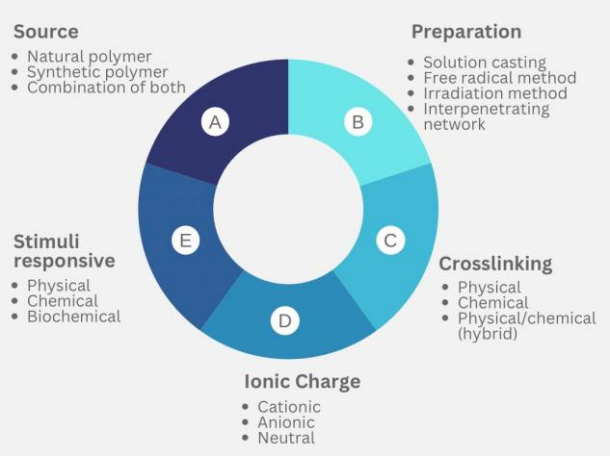

Figure 2 - Classification of a hydrogel [32].

2.4.1. Classification of Hydrogels

The following section provides a structured overview of hydrogel classification, detailing the key factors that define their properties and functionality. It addresses aspects such as polymer source, network type, crosslinking method, and crystallinity, which collectively influence the mechanical, chemical, and biological behaviour of hydrogels.

2.4.1.1. Source of Polymer

Hydrogels are primarily derived from two sources: natural and synthetic polymers. These materials are widely used in biomedical application due to their biocompatibility and biodegradability. However, despite their favourable biological properties, natural polymers often lack the mechanical strength required. Therefore, they are frequently combined with synthetic polymers to produce more durable hydrogels with mechanical properties that closely match the properties of the intended application site. Additionally, natural polymers can sometimes provoke immune or inflammatory responses when introduced into the human body [32, 33].

In contrast, synthetic polymers can be engineered and tuned to achieve mechanical properties required for specific biomedical applications. However, they are inherently biologically inert, often lacking the bioactivity needed for effective interaction with biological tissues [32, 33].

As previously mentioned, modern hydrogels are often composed of a combination of two different types of polymers to complement each other's properties. This approach typically results in superior hydrogels that combine bioactivity with adequate mechanical strength [32, 33].

2.4.1.2. Polymer Types in Hydrogels

These polymers can form hydrogels as homopolymers, copolymers, or interpenetrating networks (IPNs) [32, 33].

Homopolymers and copolymers are similar in that both are derived from a single polymer system. However, homopolymers consist of repeating units of only one type of monomer, while copolymers are composed of more than one type of monomer within the

same polymer chain. In contrast, IPNs represent a more complex structure, consisting of two distinct polymer networks crosslinked to each other [32, 33].

IPN's can be classified through 3 distinct processes of creation as seen in **Figure 3** [32, 33]:

- **Simultaneous IPNs**: Where two different polymer chains are polymerised at the same time via separate routes. Needs crosslinkers.
- **Sequential IPNs**: Where one polymer network is formed first, then a second type of monomers are polymerised within it. Needs crosslinkers.
- **Semi-IPNs**: Are a variant of Sequential IPN that doesn't need crosslinkers, where linear polymer chains are embedded in a crosslinked network.

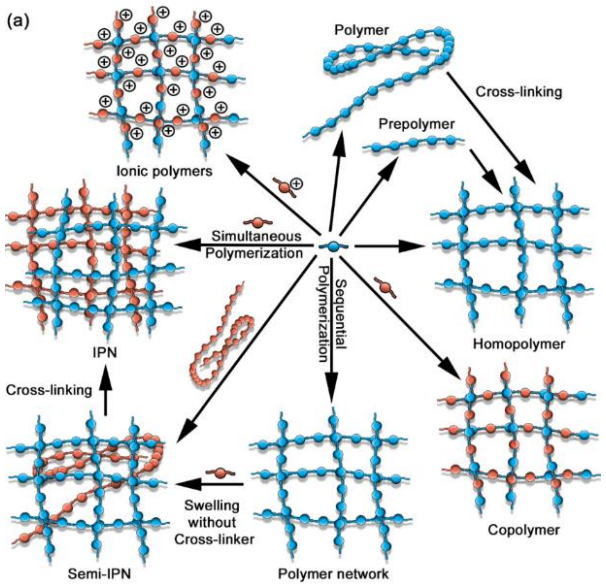

Figure 3 - Schematic representation of different types of hydrogels [33].

2.4.1.3. Crosslinking type

Hydrogels can also be classified based on the nature of the crosslinking procedure chosen to hold the polymeric network together. The procedures can be either physical or chemical processes. Physical crosslinking is a process in which the hydrogel is held together through non-covalent interactions, such as hydrogen bonds, radiation, ionic interactions, crystallization and Van der Waals forces. The crosslinked hydrogel that is a result of this process is usually weaker, although it acquires the ability to be reversible,

allowing the hydrogel to respond dynamically to stimuli like pH or temperature [32, 33]. The physical crosslinking can be performed using techniques such as cast-drying and freeze-thawing.

In contrast, chemical crosslinking involves stable covalent bonds between polymeric chains, created through chemical crosslinkers, photopolymerization or click chemistry. The hydrogels achieved through this process are more stable and mechanically resistant then the ones crosslinked through physical processes, although, they are less responsive to stimuli and can often be toxic due to the use of chemical crosslinkers [32, 33].

2.4.1.4. Polymer Ionic Charge

Hydrogels can also be classified according to the charge of their polymeric networks, which can be neutral, anionic, cationic, or zwitterionic. Neutral hydrogels, which don't possess ionizable groups, exhibit a swelling capacity mainly driven by the hydrogel's inherent hydrophilicity. Anionic and cationic hydrogels contain ionizable acidic or basic groups, respectively, which leads to pH and ionic strength-responsive swelling, making them suitable for dynamic applications. Zwitterionic hydrogels are characterised by the integration of both positive and negative charges within a single polymer, resulting in elevated hydrophilicity and antifouling properties [32, 33].

2.4.1.5. Crystallinity

Hydrogels can also be amorphous, crystalline, or semi-crystalline, which is dependent of their polymer chain organisation. Amorphous hydrogels boast randomly arranged chains, which provides a high swelling capacity. In contrast, crystalline hydrogels have more organized and tightly packed chains, which elevate its mechanical strength but limit its ability to swell. Semi-crystalline hydrogels combine both domains to achieve an adequate balance between mechanical strength and swelling capacity [32, 33].

2.4.2. PVA-Based Composite Hydrogels

Hydrogels are recurrently being studied in cartilage repair due to their ability to retain water and its viscoelastic behaviour paired with its mechanical properties. Among them, poly(vinyl alcohol) (PVA), exhibited in **Figure 4**, is one of the most researched and used polymers for its tunability, as its mechanical and structural properties can be adjusted. This flexibility allows PVA-based hydrogels to be tailored to better replicate the load bearing and lubrication of native cartilage.

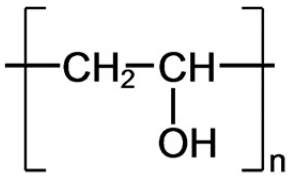

Figure 4 - Chemical structure of poly(vinyl-alcohol) (PVA) [34].

PVA is widely used in tissue engineering due to its water solubility, low cost, biocompatibility, biodegradability and favourable mechanical properties. These features make it suitable for various biomedical and pharmaceutical applications. However, in its pure form, PVA can exhibit limited stability in aqueous environments, reduced flexibility and insufficient biocompatibility and biodegradability. For this reason, PVA is often combined with other polymers or components to enhance its performance and introduce additional functional properties to the material [35].

A study on a PVA/Chitosan (CTN) hydrogel aimed to develop a biocompatible material with mechanical properties suitable for cartilage replacement. The hydrogel demonstrated a high compressive strength and a low coefficient of friction, along with good cell compatibility, indicating a strong potential for cartilage tissue engineering [36]. The chemical structure of chitosan is shown in **Figure 5**.

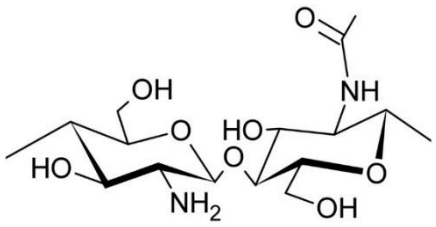

Figure 5 - Chemical structure of chitosan [37].

Similarly, Cellulose nanofibers (CNFs) in **Figure 6** have been used to reinforce PVA hydrogels. The inclusion of CNFs not only enhanced mechanical strength, flexibility and wear resistance, but also contributed to a lower coefficient of friction. The use of gamma irradiation for the crosslinking process demonstrated an improved biocompatibility by avoiding chemical additives [38].

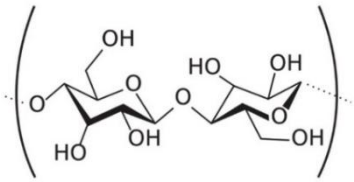

Figure 6 - Chemical structure of cellulose [39].

Another approach involves combining PVA with a calcium phosphate, such as hydroxyapatite (HAp), displayed in **Figure 7**. This composite not only presented improved mechanical stability but also exhibited osteoconductivity and biocompatibility, making it a promising option for cartilage replacement applications [40].

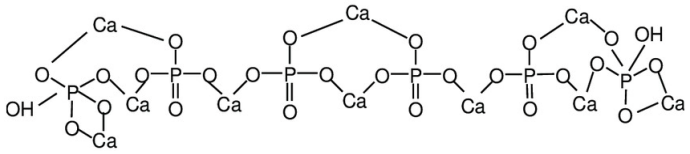

Figure 7 - Chemical structure of hydroxyapatite [41].

Finally, PVA/tannic acid (TA) composite hydrogels have shown enhanced bioadhesion and bioactivity, along with improvements in the overall mechanical performance. These characteristics are particularly advantageous for cartilage replacement [42]. The chemical structure of TA is given in **Figure 8**.

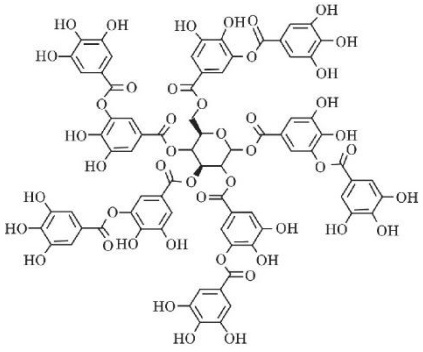

Figure 8 - Chemical structure of Tannic acid [43].

In summary, the literature demonstrates the strong potential of PVA-based composite hydrogels and highlights how the inclusion of different materials in the PVA hydrogels

matrix enables the hydrogel to be tailored into specific applications. By selecting appropriate components to combine with PVA, it is possible to enhance its mechanical strength, biocompatibility, lubrication and tissue integration.

2.5. Additive Manufacturing

Additive Manufacturing (AM) encompasses a set of fabrication techniques in which components are built in a layer-by-layer procedure, following a bottom-up approach. This method enables the efficient production of complex geometries while significantly reducing material waste compared to traditional subtractive manufacturing. In the biomedical field, AM has gained relevance ability to produce patient specific implants, tailored prosthetics and custom-made medical devices. The ability to control the geometry and the internal porosity of the developed parts facilitates tissue integration and functional performance. However, certain challenges remain, including ensuring sterilization, long-term biocompatibility, and long-term performance of the developed devices [44]. Several AM techniques are employed in biomedical fabrication, including:

- **Material Extrusion:** Structures are formed by the continuous deposition of material, extruded through a nozzle and deposited layer-by-layer [44].
- **Vat Photopolymerization:** A liquid photopolymer resin contained in a vat is selectively cured with light, solidifying the structure layer-by-layer [44].
- **Powder Bed Fusion:** A fine powder bed, is selectively fused using a laser or electron beam, producing highly precise and mechanically robust components [44].

Material extrusion is particularly interesting because it allows to easily print hydrogels, with a satisfactory geometrical precision and adjustable porosity.

2.5.1. Robocasting

Among the AM techniques previously described, Material Extrusion, particularly Direct Ink Writing (DIW), or as it is also known, Robocasting, is a technique that has emerged as one of the most suitable methods for biomedical devices production. Robocasting is an extrusion-based additive manufacturing technique in which viscous pastes, or inks, are deposited layer-by-layer through a narrow nozzle. This method enables

the fabrication of complex geometries with a tuneable porosity, making it particularly suitable for scaffold fabrication [45].

A key requirement for successful robocasting printing is the rheological behaviour of the ink, which must exhibit shear-thinning properties. This means that under high shear rates during extrusion, the ink's viscosity decreases, allowing the material to flow smoothly through the nozzle. Once deposited, the shear rate decreases and the viscosity rapidly increases, enabling the printed filament to retain its integrity and support the next layers without collapsing [45].

This technique is particularly advantageous when it comes to printing hydrogel scaffolds, because most of the hydrogel pastes already exhibit a pseudo-plastic behaviour. A study focusing on the use of robocasting to produce PVA-Based hydrogels and how the variations of paste provide different results. This study encompasses the use of distinct inks, which through the inclusion of different components can enhance the inks biocompatibility, biodegradability, mechanical performance and must importantly, printability [46].

2.6. Challenges for biomedical applications

Understanding these essential aspects is imperative for the complete comprehension of hydrogels, but to engineer effective biomedical hydrogels that are suitable for a range of applications, it is crucial to recognise and overcome specific challenges. The following section bellow intends to discuss the key issues in detail.

2.6.1. Mechanical Strength

The mechanical strength of hydrogels is an extremely important metric, considering that the hydrogels developed must replicate almost perfectly the behaviour of cartilage when facing mechanical stress. One of the most important factors regarding the mechanical strength of hydrogels is its stiffness, which will determine the longevity of the hydrogel inside the body. A study was conducted in which the performance of a hydrogel with varying stiffnesses, ranging from 1kPa, 7 kPa and 33kPa, was compared.

The results concluded that stiffer hydrogels had better results regarding its longevity and overall capacity of providing a faster regeneration of cartilage tissue, contrasting with the softer hydrogels that would be completely deteriorated after 21 days [47]. The hydrogels must be capable of good shock absorption and lubrication to protect the joint, which would be done by the cartilage if it was healthy. Despite several technological advances in this field, achieving all of this is still a considerable challenge.

2.6.2. Immune Response

When working with implantable materials, one aspect that must be seriously considered is the immune response of the body to that foreign material. One of the concerns present in this field, which is coincidentally connected to the previous sub-chapter is the fact that overly stiff hydrogels promote pro-inflammatory macrophages, while softer hydrogels favour a steadier healing [48]**.** This study considers that hydrogels must be specifically tuned according to the specific application in which they will be used.

2.6.3. Adhesion Strategies

Due to the characteristics of the cartilaginous environment, it's very challenging to ensure a secure adhesion of any material that is implanted in the cartilage, due to it being a soft tissue that is constantly under dynamic stress and presents a hydrated surface [49]. Although many strategies have been explored, there are still several pressing limitations that are yet to be resolved, such as the adhesion to wet surfaces, the stability of the connection over time and the cytotoxicity of the materials used to enhance the adhesion. [45, 46, 47].

To address these challenges, the purpose of this work focuses on developing a hydrogel composite specifically designed to serve as a platform for tissue regeneration and capable of adhering to the surrounding tissues, all while being manufactured through a 3D printing technique.

To achieve this goal, a composite polymeric scaffold will be combined with a cast-dried hydrogel to form an implant that supports cartilage repair and stimulates natural regeneration. By fusing these two layers into a hybrid hydrogel, it's possible to achieve a material where the lower layer provides mechanical strength and promotes cell adhesion

to the material, while the upper layer also contributes to adhesion but is primarily engineered to reduce friction at the cartilage-cartilage interface.

The use of 3D printing for scaffold fabrication is driven by the need for a patient-specific product, enabling each scaffold to be tailored to the exact size and geometry of the cartilage defect. In addition, the printed scaffold can incorporate a designed internal geometry, which promotes cell infiltration while maintaining mechanical strength.

3. Methods and Materials

This chapter outlines the materials, scaffold fabrication procedures, and characterization methods employed in this investigation. It provides an overview of the hydrogel composition, production techniques, and the subsequent evaluation of mechanical, tribological, chemical, and biological properties. The following sub-chapters describe each aspect in detail, highlighting how the methods support the development of hydrogels suitable for cartilage tissue engineering.

3.1. Materials

The hydrogel scaffolds developed in this study were composed of PVA (Sigma Aldrich™, USA; molecular weight 89.000-98.00 g/mol, 99-99.8% hydrolysed), chitosan (Sigma Aldrich™, USA; degree of deacetylation ≥ 75%), cellulose nanofibers (NanoGrafi, Turkey; average molecular weight 20.000 g/mol), and hydroxyapatite (Sigma Aldrich™, USA). For the upper layer, tannic acid (Sigma Aldrich™, USA) was incorporated into the PVA matrix. For the tribological assay, plugs (8 mm diameter) were harvested from a femoral porcine articular cartilage and synovial fluid was used as the lubricant.

Regarding the biological assay, for the subculture preparation, MG63 osteoblast-like cells (CRL1427™, ATCC) were cultured in Eagle´s Minimum Essential Medium (EMEM, Sigma Aldrich™, USA) supplemented with Fetal Bovine Serum (FBS, Sigma Aldrich™, USA) and a Penicillin-Streptomycin solution (Sigma Aldrich™, USA; 10000 U/mL penicillin and 10 mg/mL streptomycin). Cells were detached using trypsin-EDTA (Sigma Aldrich™, USA). For the viability assay, MTT (Sigma Aldrich™, USA) and a solvent containing hydrochloric Acid (HCL, Sigma Aldrich™, USA), IGEPAL (Merck, Germany) and isopropanol (Sigma Aldrich™, USA) were used. Finally, for the cell adhesion assay, glutaraldehyde (Merck, Germany) and a cacodylate buffered solution (PanReac AppliChem, Spain) were employed.

3.2. Sample Production

3.2.1. Scaffolds

The polymeric scaffolds were synthesized via a robocasting procedure and consisted of a multi-component mixture.

The polymeric scaffolds were synthesized through a robocasting procedure and contained a mix of components. A solution of 1.77g of PVA, 0.33g of hydroxyapatite and 7.25g of water was developed. The mixture was then incubated at 90ºC for 24h to ensure complete dissolution of PVA and a homogenous dispersion of hydroxyapatite.

After the initial PVA-HAp suspension was dissolved, an additional 0.2g of HAp was added, followed by 0.55g of Chitosan and 0.14g of Cellulose nanofibers (0.14g). The final composite concentrations are as follow in **Table 3**:

Table 3 – Mass percentage of the ink components.

	wt%
PVA	17.3
HAp	5.2
Chitosan	5.4
CNFs	1.4
H_2O	70.8

The suspension was cooled to room temperature (RT) before being loaded into a syringe with a 0.61mm inner diameter blunt-edged dispensing tip (BENECREAT, China). The syringe was then mounted onto a food 3D printer (ByFlow Focus, ByFlow, Netherlands), and polymeric paste was deposited via robocasting into hollow rectangular sample developed using a Computer Assisted Design (CAD) with the OnShape Software and subsequently sliced in PrusaSlicer Software. Using PrusaSlicer, sample dimensions (10mm x 10mm x 4mm) and printing parameters such as extrusion speed (1 to 4 mm/s, which varied with the layer being printed), the nozzle size (0.60/0.65 mm) and the sample's infill (50%) were adjusted to match the intended physical size, as illustrated in

Figure 9. After printing, the scaffolds were left to dry at RT until fully solidified. The resulting scaffold samples are referred to as SC.

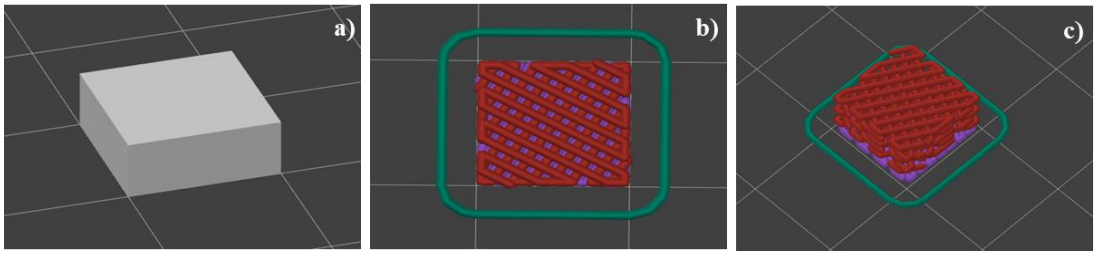

Figure 9 - (a) Unprocessed 3D model (raw design); (b) geometry slice [top view]; (c) 3D scaffold model with solid base.

3.2.2. Upper Layer

For the upper layer, three types of PVA discs with varying tannic acid concentrations were prepared. First, 15 wt% PVA solutions were prepared, to which tannic acid was added at 0%, 1% or 3 wt% to obtain distinct PVA/tannic acid mixtures. These solutions were then incubated at 90º C for 24h. After incubation, each sample was poured into Petri dishes and promptly covered with a perforated film to allow slow and consistent cast-drying at RT. Condensation was removed periodically throughout the drying process. The resulting upper layer samples were labelled 0T, 1T and 3T, corresponding to increasing tannic acid concentrations.

3.2.3. Bi-Layer Scaffold

The bi-layer scaffold was prepared following the procedure described in the previous section. First, 3T PVA/tannic acid discs where produced. During the drying process, pre-hydrated scaffolds were deposited onto the surface of the 3T layer after 3h. The combined sample was then air-dried at RT until fully solidified. The resulting bi-layer scaffold is designated as 3TSC. All scaffold, upper layer and bi-layer samples, that underwent gamma irradiation, are indicated with an “R” in their identification.

3.2.4. Post Processing

Once fully dried, all sample types were subjected to a standardized washing protocol comprising of five 24-hour cycles on an orbital shaker at 120 rpm. Following each cycle, the wash solution was replaced with fresh deionized water to ensure a proper pH stabilization of the printed samples. Subsequently, all samples intended for

biocompatibility testing werr sterilized by gamma irradiation at a total dose of 29 kGy, applied at a dose rate of 5kGy/h.

3.3. Characterization

3.3.1. Rheological Behaviour

The rheological behaviour of the hydrogel paste was evaluated through an MCR-92 Modular Compact Rheometer (Anton Paar, Austria), using 50 mm geometry and a measuring interval of 0.1mm. Viscosity was determined in an interval between 0.1 – 1000 s^{-1}, at 25ºC. The assay was conducted in triplicate.

3.3.2. Morphology

The morphology of the hydrogels was analysed at both the macro- and microscale. Macroscale analysis was performed using a Zoom 2000 Stereozoom Microscope (Leica, Germany) with a magnification range of 7 – 15x. For detailed microscale analysis, a scanning electron microscope (SEM) was conducted at an acceleration voltage of 15kV using a a Phenom XL G3 Desktop SEM (Thermo Fisher, USA). Surface morphology was assessed for hydrogel scaffolds, bi-layer scaffolds, and samples with adhered cells, as well as the cross-section morphology of the upper layer samples with varying concentrations.

Prior to imaging, all samples were dehydrated through sequential immersion in ethanol solutions of increasing concentration (50%, 75%, 90% and 95%) for 10 mins each, then dried in an incubator at 40ºC for 24h and stored in airtight containers to prevent moisture accumulation. For the cross-section analysis, upper layer samples were immersed in liquid nitrogen for 10 seconds and immediately fractured. Due to their lack of conductivity, all prepared samples were coated with a gold-palladium conductive layer to facilitate SEM imaging.

3.3.3. Chemical Analysis

Fourier-transform infrared (FTIR) spectroscopy was employed to analyse the chemical structure of the materials. This technique is particularly useful for detecting

chemical changes caused by material interactions or processes such as gamma-ray sterilization [15].

Prior to analysis, all samples were dried at 40ºC to ensure adequate removal of any residual water or humidity. FTIR spectra were acquired using a Spectrum Two™ FT-IR Spectrometer (PerkinElmer, USA), equipped with a Quest High Throughput ATR accessory (SPECAC, UK). Measurements were performed over a range of 4000-500 cm^{-1}, with a resolution of 1 cm^{-1}, averaging six scans per sample.

3.3.4. Water Content

Hydrogels are regarded as promising candidates for cartilage replacement due to their three-dimensional hydrophilic polymer network, that not only allow to effectively absorb water while maintaining structural integrity. The swelling capacity of hydrogels is directly correlated to their degree of crosslinking, although it can also be influenced by external factors such as temperature and pH [15]. This swelling behaviour, paired with the hydrogels mechanical properties is truly valuable to tissue engineering, because it allows to closely mimic the native tissue.

For this study, circular samples (8 mm diameter) were extracted from the hydrated scaffolds, upper layer discs and bi-layer constructs using a circular cutter. Sample wet mass was determined using a semi-micro analytical balance (A&D Instruments, GR-200-EC) following a blotting procedure, in which excess surface water was gently removed without deforming the specimen. The samples were then dried in an incubator at 40ºC until a constant mass was achieved and weighed again.

To estimate the equilibrium water content (EWC), the following equation was used:

$$EWC(\%) = \frac{\mathrm{W_h} - \mathrm{W_d}}{W_h} \times 100 \quad (1)$$

Where W_d represents the weight of the dried sample and $\mathrm{W_h}$ represents the weight of the hydrated samples. For each sample, five independent measurements were performed.

3.3.5. Mechanical Properties

Understanding the mechanical behaviour of the hydrogel scaffold is crucial, given their intended function in articular cartilage replacement. Articular cartilage subjected to continuous mechanical loading, and therefore, the developed hydrogels must be capable to support compressive forces while maintaining long-term structural ability. The mechanical properties of the samples were evaluated through the stress/strain curve resultant from an unconfined compression test, which employed a cylindrical disk, to ensure uniform load distribution [15].

The unconfined compressive tests were performed in deionized water, using a TA.XT Express Texture Analyser (Stable Micro Systems, UK) at RT. Prior to each measurement, a 2 N pre-load was applied. The samples had a diameter of 8mm and variable thicknesses, ranging from 0.82-2.98 mm, and for each sample type, 5 measurements were made. Compression was applied using a 49 N load cell at a strain rate of 0.5mm/s until the maximum capacity of the force sensor (5kg) was reached. The unloading was performed at the same rate, and the entire test cycle was monitored.

From the resulting stress-strain curves, the tangent compressive modulus was determined between the strain range of 5% to 20%, in 5% increments, using following equation:

$$E_t = \frac{\sigma_{\varepsilon+\Delta\varepsilon} - \sigma_{\varepsilon-\Delta\varepsilon}}{2\Delta\varepsilon} \quad (2)$$

Where the difference is strain value Δε was 1%.

3.3.6. Tribological Assessment (Friction)

Tribology is defined as the science and technology behind the study of friction, wear and lubrication between interacting surfaces [53]. In this study, the tribological testing was performed to evaluate whether the material drafted to compose the upper layer was adequate to substitute articular cartilage.

A TRB^3 tribometer (Anton Paar, Austria) was used with a pin-on-plate configuration at RT, with synovial fluid harvested from human donors as a lubricant. The testing

parameters consisted in 1200 cycles, with a 6 mm full amplitude linear movement, frequency of 1 Hz (which is close to the reported frequency for typical adult walking speeds [54]) and normal load of 50 N which allowed to simulate a realistic walking scenario. As a counterbody, porcine articular cartilage plugs (8 mm diameter) were used against PVA/tannic acid samples with varying degrees of tannic acid concentration. Due to the difference in diameter between the PVA samples and the cartilage plugs, three replicate measurements were performed for each sample group.

The friction curves were obtained through the InstrumX software, which allowed to calculate the coefficient of friction (CoF). The pressure (P) was also determined. Both were calculated with the following equations:

$$\mu = \frac{F_T}{F_N} \tag{3}$$

$$P = \frac{F}{A} \tag{4}$$

Where μ is the CoF, F_T is the frictional force and F_N is the normal load for the coefficient of friction, while F is force and A is area for the pressure.

3.3.7. Biological Assay

Because the developed hydrogel is intended for the use in tissue engineering, it must support and promote cell growth, without being harmful to previously existing tissue. Therefore, both cell viability and cell adhesion were evaluated.

Subculture Preparation

MG63 osteoblast-like cells were used for the viability and adhesion assays. Cells were cultured in EMEM supplemented with heat inactivated FBS until a final concentration of 10% and 1% antibiotics. Cells were then incubated at 37ºC in a humidified atmosphere containing 5% CO_2. For subculture, cells were detached using a trypsin-EDTA 1 x solution, centrifuged, resuspended in fresh medium, and counted with a hemocytometer.

Viability

Extracts from the hydrogels samples were prepared according to the ISO 10993-12 guidelines [55]. Samples were immersed in supplemented EMEM in falcon tubes at a ratio of 0.2g/mL for 24h at 37ºC in a humidified 5% CO_2 atmosphere. Additional medium was added to compensate for hydrogel swelling.

MG63 cells were seeded (1 x 10^4 cells/well) in a 96-well plate and incubated at 37ºC in a humidified 5% CO_2 atmosphere for 24h. The cell seeding was performed in 5 replicates for each of the following groups: 1:1, C+ (Positive control with 5% DMSO in the medium), C- (Negative control with only culture medium).

After incubation, the medium was replaced with 100 µL of the respective sample extract and incubated for an additional 24h. The extracts were then aspirated, and the cells were washed with Phosphate-Buffered Saline (PBS). Subsequently, MTT solution dissolved in serum-free EMEM at a concentration of 0.5 mg/mL was added to each well and incubated for 3h. Formazan crystals formed during the MTT assay were dissolved using a solvent of 4 mM HCL and 1% IGEPAL in isopropanol. The 96-well plate was agitated for 15 min to ensure an even dissolution of formazan crystals before the absorbance was read at 565nm in a microplate reader (Infinite M Plex, Tecan, Switzerland). The quantification of cell viability was normalized to the negative control.

Adhesion

Sterilized (gamma-irradiated) scaffold samples were placed into well plates and rehydrated in supplemented EMEM for 1h at 37º C and 5% CO_2. Following rehydration, the medium was aspirated, and MG63 (1 x 10^4 cells /sample) were carefully seeded onto each scaffolds surface. The samples were returned to the incubator for 1 hour to allow cell attachment, after which fresh EMEM medium was added and incubation continued for an additional 19h under the same conditions. Post-Incubation, the culture medium was removed, and the samples were fixed with 3% glutaraldehyde in 0.1M cacodylate buffer (pH 7.3), followed by washing with the same buffer.

4. Results

4.1. Rheologic Behaviour

By analysing the rheological data presented in **Figure 10**, it's evident that the printable paste exhibited pseudoplastic (or shear-thinning) behaviour. This is corroborated by the curves trajectory, whereas the shear rate increases, the viscosity drastically decreases, indicating that the material flows easily under shear stress.

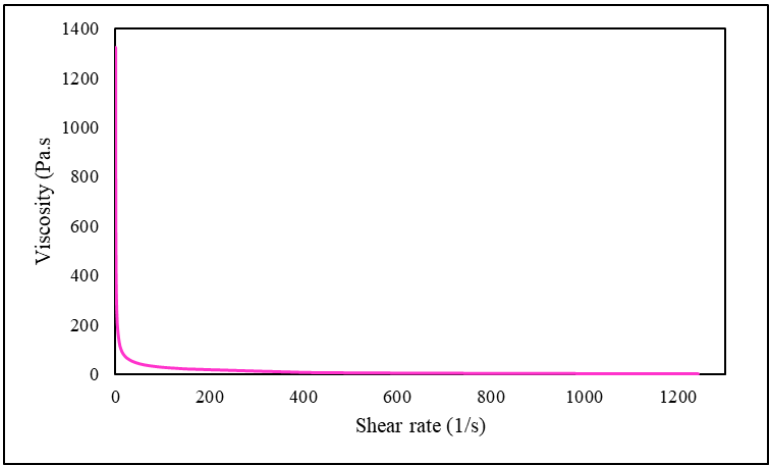

Figure 10 - Rheological characterization of the printing paste.

4.2. Morphology

Macroscale analysis of the scaffold morphology revealed the high precision of the filament deposition process, where the paste filaments were uniformly layered to form a mesh-like geometry. This geometry was intentionally designed to achieve both mechanical stability and biological function. The symmetric and interconnected structure provides adequate structural resistance while promoting cell adhesion and proliferation through its inherent porosity.

Observation of the upper-layer samples further complemented the macroscale findings with two key characteristics: its brown colouring, which indicates the successful incorporation of tannic acid within the PVA matrix, and the predominantly smooth surface.

Additionally, the bi-layered scaffolds exhibited a distinct stratified morphology, consisting of a lower mesh-like layer and an upper smooth layer, where the previously hollow and well-defined mesh-like geometry is completely impregnated with PVA. Representative examples of the samples analysed at the macroscale level are shown in **Figure 11**.

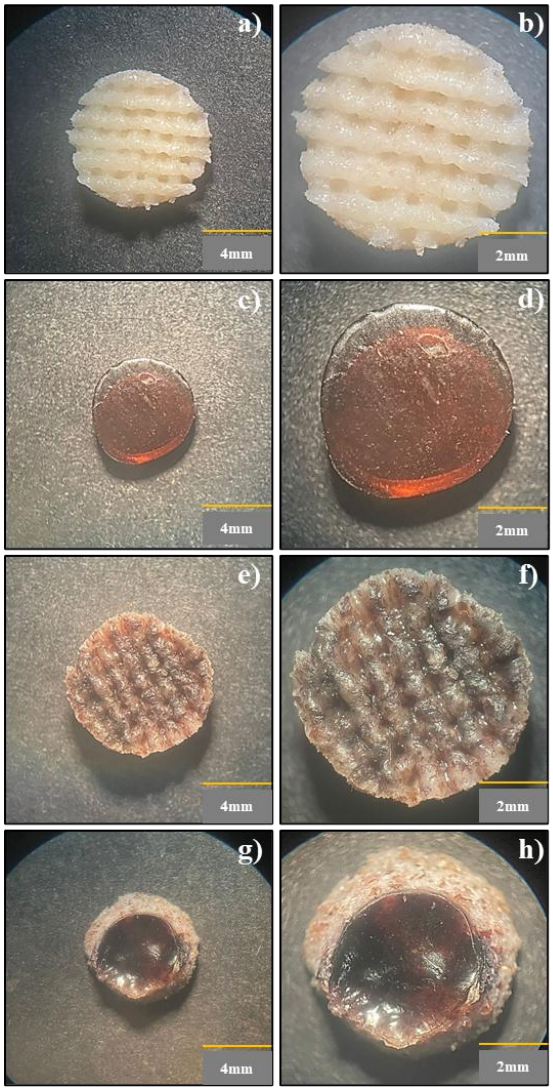

Figure 11 - Macroscale analysis of the three sample types - (a, b) SC; (c,d) 3T; (e, f) 3TSC scaffold; (g, h) 3TSC upper layer.

Microscale observation of the previously mentioned samples, plus the sample for cell adhesion are represented in **Figure 12**. The SC samples exhibited a rugged surface, where it is clearly visible the differentiation between layers. Another observed characteristic is the fact that the samples presented small imperfection in the surface, further increasing the already rough surface. Further EDS (Energy-dispersive X-ray spectroscopy) analysis (coupled to the SEM and represented in **Figure 12**) revealed that the small white particles scattered around the surface of the SC samples consisted of HAp particle, as it was determined by the high concentration of calcium in its composition.

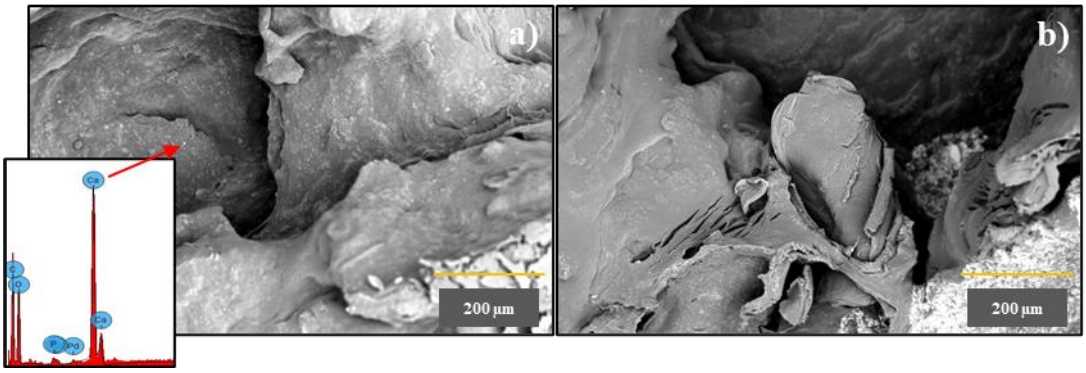

Figure 12 - Microscale analysis of the SC sample surface with supplementary EDS analysis.

3TSC samples, represented in **Figure 13** exhibited smoother surfaces when compared with the previous samples. By observing the hollow regions of the bi-layer scaffold, it is apparent that all the surface inside the cavity has been coated with the 3T hydrogel.

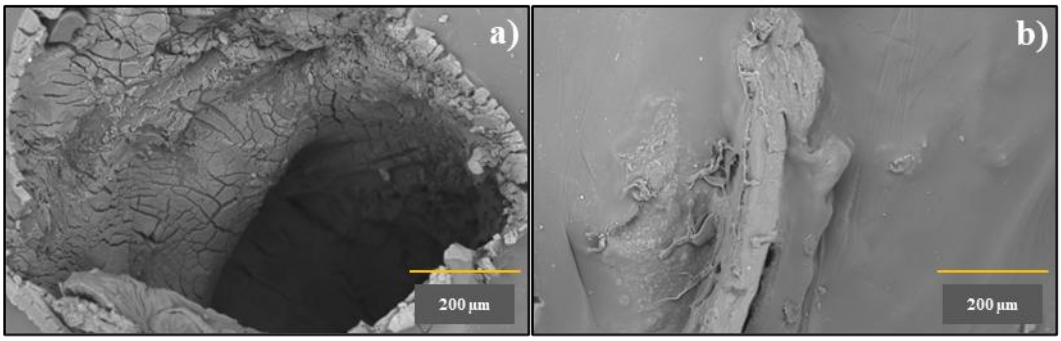

Figure 13 - Microscale analysis of the 3TSC sample (cavity and surface).

Furthermore, the cross-section analysis of 0T, 1T and 3T samples in **Figure 14** demonstrated that all hydrogel types presented a uniform structure without inner porosity.

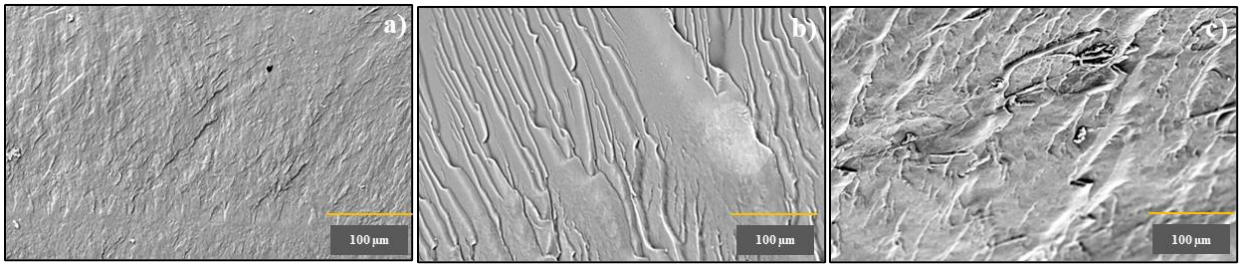

Figure 14 - Cross-section analysis of 0T,1T and 3T samples.

4.3. Chemical Analysis

To evaluate the chemical structure of the upper layer and determine potential interactions between PVA and TA, FTIR spectroscopy was performed. The spectra of pure PVA and PVA-based hydrogel exhibited the typical characteristic peaks: a broad O-H stretching band between 3200-3400 cm^{-1}, C-H stretching around 2920-2940 cm^{-1} and the crystallinity associated bands in 1140-1080 cm^{-1} region [56]. In contrast, the pure TA spectra features a very broad O-H band, that strongly overlaps with PVA, a prominent carbonyl/ester-like band near 1700-1730 cm^{-1}, distinct aromatic ring vibrations within the 1610-1510 cm^{-1} region and phenolic C-O bands around 1300-1200 cm^{-1} [52, 53]. When the spectra of the upper layers are compared to those of the individual components it's evident that the overall spectral profile remains dominated by PVA. The 0T sample is essentially superimposable with pure PVA, with no significant differences in its chemical structure. However, in the 1T and 3T samples, a small peak starts to form and gradually increases with tannic acid concentration in the 1610-1510 cm^{-1} signifying successful incorporation of TA into the upper layer [57]. However, due to the absence of new peaks in the upper layers chemical signature, it is possible that the inclusion of TA is merely due to a blend and not dependent of any strong chemical interaction between components, as represented in **Figure 15**.

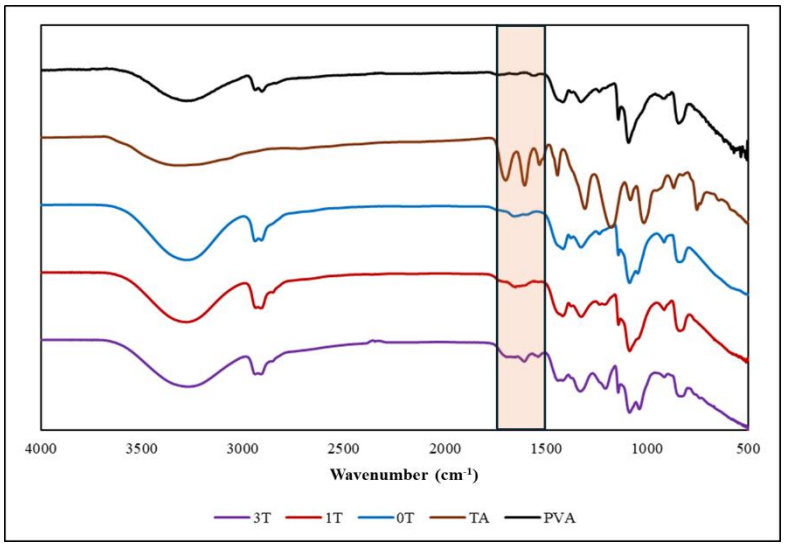

Figure 15 - FTIR spectra of PVA/tannic acid hydrogels.

The same FTIR approach was applied to confirm the incorporation of the organic components of the scaffold (SC), which contained PVA, chitosan (CTN) and cellulose nanofibers (CNFs). After accounting for the dominant PVA spectral features previously described, the characteristic absorption bands of chitosan could be identified, although with a lower intensity, specifically in 1654 cm^{-1} and 1588 cm^{-1}, corresponding to the amide I band and the amide II band, respectively [59]. Evidence of CNFs was also detectable in the 1200-1020 cm^{-1} region, which corresponds to the C-O and C-O-C stretching vibrations. In combination with the chitosan contribution, these signals result in the appearance of a distinct peak centred at 1031 cm^{-1}, consistent with cellulose-based materials [60]. However, once again no new peaks or significant band shifts associated with CNFs were detected, suggesting that their involvement is derived from its physical dispersion rather than strong chemical interaction with the other components of the composite, as illustrated in **Figure 16**.

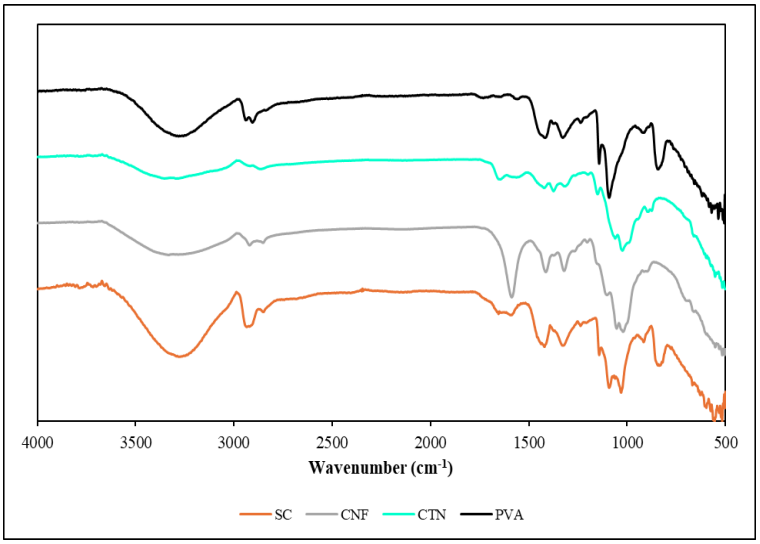

Figure 16 - FTIR spectra of scaffold samples.

The bi-layer scaffold was also analysed to assess whether any chemical interaction occurred between the scaffold matrix and the upper hydrogel layer. When compared with the (SC)R sample, the spectrum of the (3TSC)R sample shows an additional weal shoulder appearing at the 1634 cm^{-1} band, corresponding to the aromatic ring vibrations characteristic of TA. This feature is also present in the (3T)R spectra, confirming that TA is present in the scaffold. Furthermore, the appearance of a new signal at 1200 cm^{-1} can be attributed to phenolic C-O stretching, which is typically associated with TA. Together, these spectral features indicate that TA became integrated within the scaffold matrix, as illustrated in **Figure 17**.

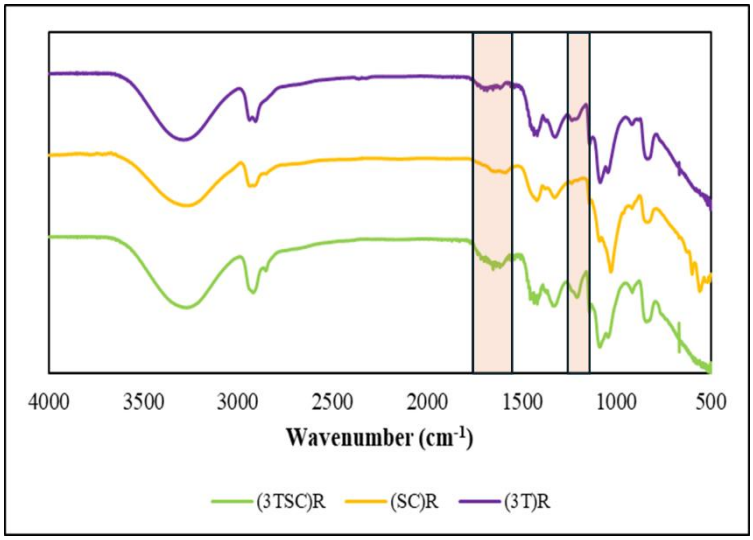

Figure 17 - FTIR spectra of bi-layer (3TSC)R sample.

The effect of gamma irradiation on the chemical structure of the materials was assessed through FTIR analysis. Both the upper layers containing TA (1T and 3T) and the scaffold (SC) were examined to determine whether irradiation induced any chemical modifications. As shown in **Figure 18**, the comparison between 1T vs (1T)R and 3T vs (3T)R reveals a noticeable broadening of the O-H band in the 3200 cm^{-1} regions along with a smoothening and slight reduction in definition of the aromatic signals associated with TA near 1650 cm^{-1}. These spectral changes are consistent with hydrogen-bond network reorganization and the irradiation-induced crosslinking, as well as mild oxidative effects that lead to partial decrease in the structural ordering [60, 61].

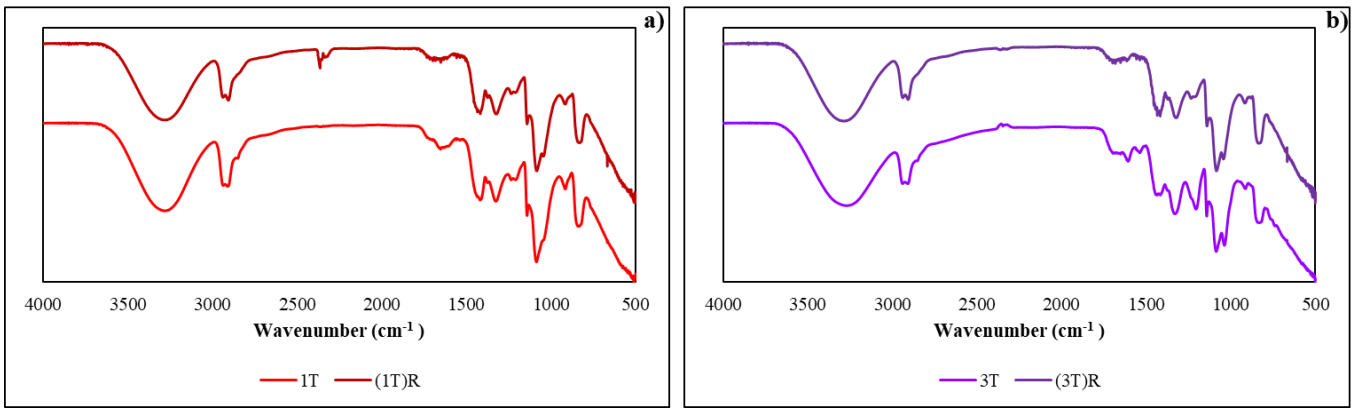

Figure 18 - Effects of gamma radiation in PVA/tannic acid hydrogels: (a) 1T; (b) 3T.

For the scaffold samples, similar irradiation-induced spectral modifications were observed. A broadening of the O-H stretching band in the 3200 cm^{-1} is evident, along with a smoothening of the 1580 – 1660 cm^{-1} region, which corresponds to the amide I and amide II vibrations of chitosan. Additionally, a reduction in the intensity of the PVA crystallinity region (1140-1080 cm^{-1}) was detected. This decrease is characteristic of the reduced crystalline organization within semi-crystalline polymers. Gamma irradiation generates free radicals along the PVA backbone, which subsequently recombine to form covalent crosslinks, restricting chain mobility. The formation of these inter-chain bonds disrupts ordered packing, thereby lowering the degree of crystallinity, as shown in **Figure 19** [56, 58]**.**

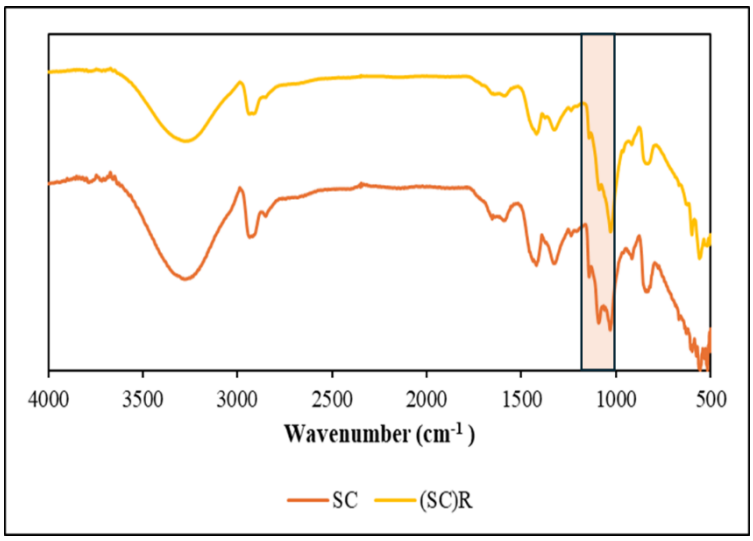

Figure 19 - Effects of gamma radiation in SC samples.

4.4. Water Content

Illustrated in **Figure 20** are the results of the equilibrium water content (EWC) analysis for both irradiated and non-irradiated samples. In the scaffold samples, the non-irradiated specimens exhibited a higher EWC value, indicating that gamma irradiation reduced their ability to absorb and retain water.

However, despite exhibiting a small difference, the upper layer hydrogel samples exhibited a contrasting behaviour for the irradiated variants, which displayed higher values of EWC. These variations are likely referent to batch-related structural heterogeneity, such as differences in porosity. While the scaffold samples exhibited an expectable result due to the possible crosslinking derived from gamma irradiation affecting the scaffolds porosity, the upper layer samples display a heterogenous behaviour.

Another comparison was made between the irradiated scaffold ((SC)R) and the irradiated bi-layer scaffold ((3TSC)R), also shown in **Figure 20**. As expected, both the EWC and the SC were lower in the (3TSC)R samples. This reduction is attributed to the penetration and the absorption of the PVA-based upper layer into the scaffold's matrix, which partially occupies the scaffold's pore network, reducing its water uptake.

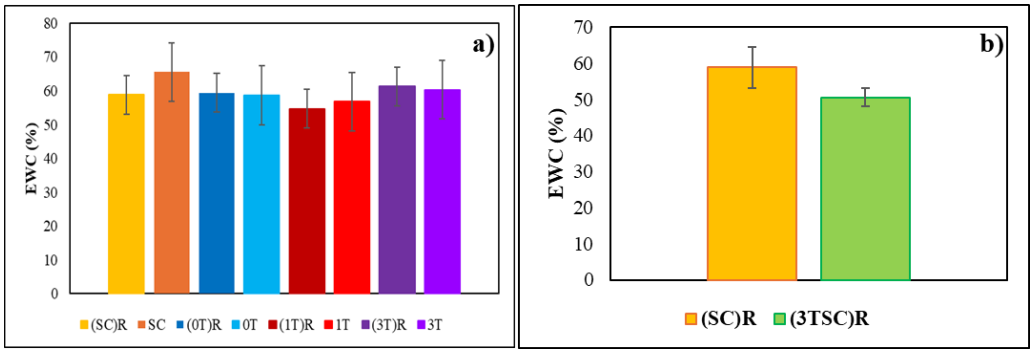

Figure 20 - Water content analysis of irradiated and non-irradiated: (a) scaffold and upper layer samples; (b) scaffold vs bi-layer samples.

4.5. Mechanical Properties

The mechanical performance of all sample types, both irradiated and non-irradiated, was evaluated through compressive testing. From these tests, the typical compressive stress-strain curves, and the corresponding tangent compressive moduli were obtained and are presented in **Figure 21** and **Figure 22**.

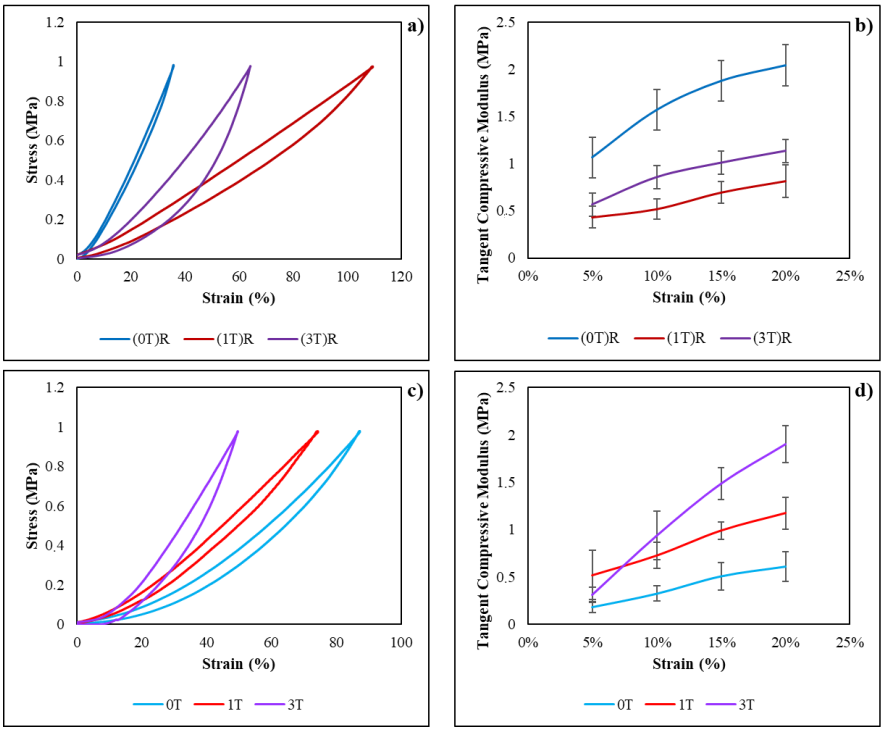

Figure 21 - Typical compressive stress-strain curves and tangent compressive modulus of PVA/tannic acid hydrogels: (a, b) irradiated; (c,d) non-irradiated.

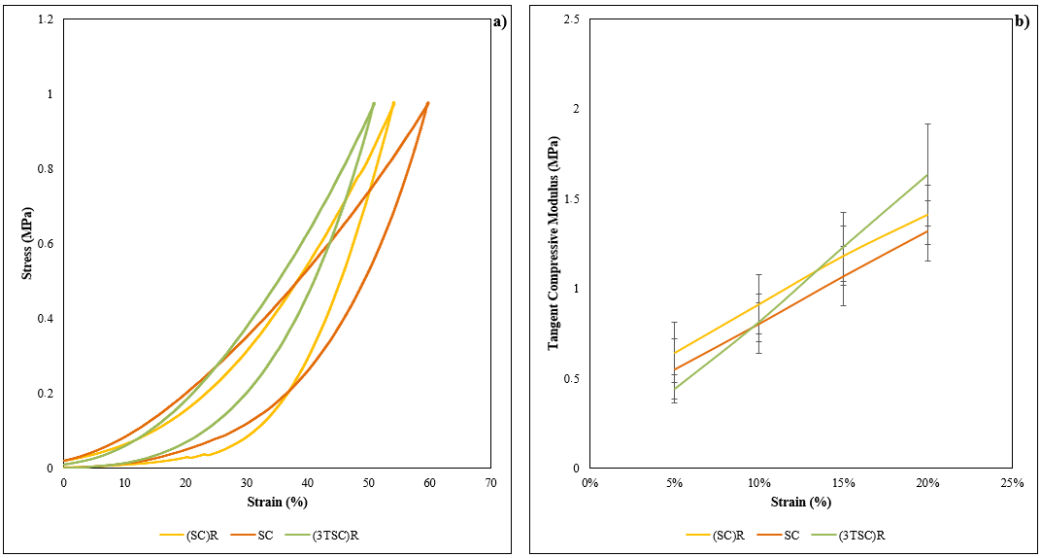

Figure 22 - Typical compressive stress-strain curves and tangent compressive modulus of irradiated and non-irradiated scaffold samples and bi-layer sample.

In general, all samples subjected to compression exhibited similar overall behaviour. As the applied stress increased, a corresponding increase in deformation was observed. However, the response was non-linear and characteristic of viscoelastic materials.

For the upper-layer samples, the stress-strain curves for the non-irradiated groups followed the expected trend: increasing tannic acid concentration resulted in greater resistance to deformation. In contrast, the irradiated samples displayed the opposite behaviour, where the presence of tannic acid was associated with reduced mechanical performance compared to the pure PVA samples.

The scaffold samples demonstrated a more uniform trend. Although the irradiated scaffolds and the bi-layer samples showed slightly higher mechanical values, the increase was not substantial. Finally, when comparing the upper-layer samples to the scaffold samples, the upper-layer consistently exhibited higher tangent compressive moduli values, which can be attributed to the greater porosity and structural hollowness of the scaffold architecture.

4.6. Tribological Assessment

The tribological assays helped to assess the CoF (coefficient of friction) of all upper-layer samples. Results suggested that all three sample types moved swiftly to a steadier friction value. While for the (0T)R samples the trajectory is ascending, which reflects an increase in the CoF, the other two samples, (1T)R and (3T)R start at a higher CoF value but decrease rapidly, as it is represented in **Figure 23**. For the applied normal load of 50N acting over an area of ~ 5.03 x 10^{-5} m^2, the resulting pressure was ~ 1 MPa. This value is consistent with pressures reported for articular cartilage under physiological loading conditions. Previous studies have reported average hip joint contact pressures of approximately 0.7 MPa, with cartilage stresses during walking ranging from 0.1 to 4 MPa [64]. These reported values encompass the pressure obtained in the present analysis

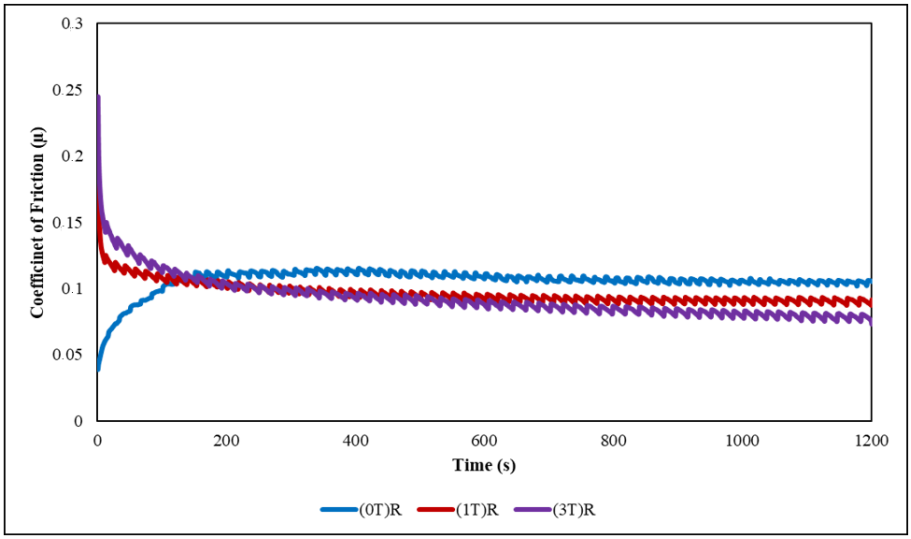

Figure 23 - Coefficient of friction of PVA/tannic acid irradiated samples.

4.7. Biological Assay

Viability

Cellular viability was also assed. The results obtained regarding the MTT assay revealed that the SC samples exhibited excellent results, where the percentage of healthy cells comparatively to the C- control was close to 98%, has demonstrated in **Table 4.**

Table 4 - Cell viability assay results.

%	SC	C-	C+
1	99,60	88,65	68,54
2	97,26	101,45	47,32
3	98,53	101,97	48,57
4	92,96	102,99	54,42
5	99,30	104,91	55,74
Average	97,53	100	54,92

Adhesion

Regarding the cell adhesion assay, a comparison of the scaffolds surface before and after cell seeding shows a clear change in the surface morphology. Areas that before presented a limited ruggedness now present elevated features and small cavities, indicating the attachment and spreading of cells on the scaffold surface. The observations are illustrated in **Figure 25**.

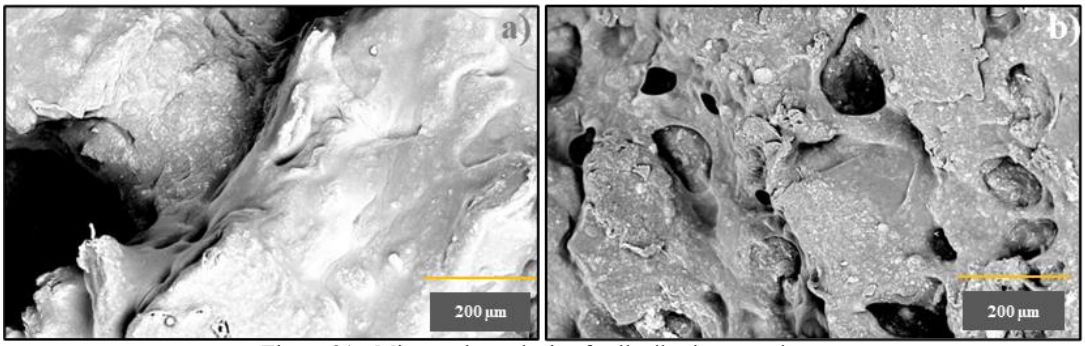

Figure 21 - Microscale analysis of cell adhesion samples.

5. Discussion

The objective of the present study was to fabricate a bilayer material designed to enhance the anchorage of the hydrogel to the subchondral bone. For this end, scaffolds enriched with chitosan, HAp particles and cellulose nanofibers were produced via robocasting. Those scaffolds were produced through an iterative process. The development of the paste began with a simple PVA-chitosan mixture in which PVA concentration was adjusted between 15-30%. Chitosan was chosen as the material to pair with PVA due to its biocompatibility, flexibility and antimicrobial activity [65]. Low PVA concentration produced a paste that was overly liquid, whereas higher PVA concentration resulted in excessive viscosity, making 20% PVA the most adequate baseline.

Despite this optimization, the paste remained too fluid, leading to the introduction of hydroxyapatite (HAp) in small quantities to increase viscosity. Incorporating Hap into the mixture improves the hydrogel's mechanical stability and functional performance, while additionally providing high cell-adhesive and osteoconductive properties [66]. This addition improved consistency but introduced new issues: the paste became slightly too viscous and grainy, and due to shear-thinning during extrusion, the viscosity decreased under stress, compromising the filament's stability. Increasing HAp content enhanced physical integrity but caused frequent filament breakage and nozzle clogging, prompting the addition of sorbitol to improve flexibility and printability.

A 24-hour hydration period was introduced to promote complete polymer interaction, but this caused the paste to become sponge-like, dry, and non-homogeneous due to excessive water loss overnight. The issue was resolved by introducing chitosan, HAp, and sorbitol on the same day the PVA solution was completed. A more functional formulation was obtained using 20% PVA, 3.3% HAp, 5.5% chitosan, 0.5% sorbitol, and a new addition of cellulose nanofibers. The incorporation of CNFs is widely recognized

for enhancing the mechanical strength, flexibility, and water retention capacity of PVA-based hydrogels, owing to their strong hydrogen-bonding interactions within the polymer networks [66, 67]. This version enabled the fabrication of structurally acceptable scaffolds.

For a material to be suitable for implantation, it is crucial that it is free of harmful microorganisms. Various sterilization methods can be employed to achieve this. In this study, the biomaterials were sterilized via gamma radiation, which preserves the physical integrity of the samples and has been shown that gamma radiation has a beneficial impact in the crosslinking of certain hydrogels, strengthening the bonds between the polymeric chains [69].

Subsequent cytotoxicity tests revealed that the material was not biocompatible (has seen in **Table 5** in the **Appendix A** section, killing most of the cultured cells due to an acidic pH traced to sorbitol, which is known to degrade into simple acids under gamma irradiation, incited its removal from the paste composition. A study detailed how gamma irradiation is responsible for the formation of new carbonyl and carboxyl signals in a carbohydrate system consistent with oxidation [70], while another study identifies formic, acetic and other carboxylic acids as major sugar degradation products [71].

Autoclave sterilization was briefly experimented on the scaffolds, however it proved to be damaging to the samples due to heat and moisture, which further indicated that gamma irradiation was the optimal sterilization method. The resulting sorbitol-free formulation became the final base material described in Section 3. Two additional variations were developed as potential alternatives: 1- half of the HAp in the SC samples was replaced by MgO to study a possible osteoinductive activity between the scaffold and the bone surface [72]; 2- SC samples that were annealed to reduce particle release by increasing PVA crystallinity [73]. All samples were subjected to a 24-hour washing cycle repeated over five days before further evaluation of cytotoxicity. Both variations were ultimately discarded: the samples containing MgO exhibited a harmfully high pH (9), while the annealed samples showed no improvement in cell viability and demonstrated inferior water absorption properties.

Due to the structural design of the bi-layer scaffold, it was necessary to incorporate an upper layer that would serve as the primary interface between the implant and the

native cartilage. Achieving a reliable adhesion between implanted biomaterials and the surrounding tissues is a well-known challenge in tissue engineering, as insufficient interfacial bonding can compromise the integration and the long-term performance of the implant. To address this, tannic acid was selected as the adhesive component. Tannic acid offers excellent biocompatibility and demonstrates strong adhesive behaviour, making it a suitable candidate for enhancing scaffold-tissue interaction [72, 73]. To achieve this, multiple 3T samples, that were composed of a PVA/tannic acid mixture, were poured into small Petri dishes, where the addition of the scaffold samples to the 3T mixture was made when the viscosity was sufficiently high to prevent the scaffolds from sinking. In a tribomechanical perspective, tannic acid was added in the upper layer system to improve the mechanical performance of the upper layer, as well as decreasing its coefficient of friction [76]. Two insertion methods were tested: direct insertion and partial insertion. In direct insertion, the SC samples were placed directly onto the 3T surface. For the partial insertion method, the SC samples were gently lowered using four needle tips in each of the samples' corners, ensuring that only the bottom surface contacted the 3T layer. However, direct insertion proved to be the most effective method, as partial insertion consistently produced air pockets due to uneven drying.

The analysis of the fabricated samples revealed several important questions that require additional clarification to fully understand the underlying mechanisms of the 3D printed composite bi-layer hydrogel.

The water content analyses provided important insights into the effects of gamma irradiation on the developed samples. As observed in Section 3, most irradiated specimens exhibited a clear decrease in EWC. At first sight, this reduction could be considered beneficial, as lower hydration generally correlates with increased hydrogel stiffness. However, reduced water content also compromises lubrication. One study reported that increased stiffness can lead to pore collapse and further water loss, ultimately contributing to an increase in the CoF of the material [77].

When compared to native articular cartilage, the bi-layer scaffold samples showed EWC values slightly below the physiological range. The measured EWC of ~50% contrasts with the natural AC values typically reported around 70–80% [78].

Most PVA hydrogel scaffolds developed for cartilage tissue engineering can mimic the high-water uptake of native cartilage. Several studies report EWC values ranging from 70% to over 80% in similar scaffolds, which closely matches natural AC hydration levels [77, 78]. A key differentiating factor in the present work, however, is the use of gamma irradiation, which has been shown to reduce the intrinsic EWC of hydrogels [78].

These findings help contextualize the mechanical and tribological behaviours observed. Typically, drier hydrogels exhibit better performance in compression due to their higher stiffness, whereas their reduced flexibility and diminished fluid support lead to an inferior tribological performance.

When analysing the scaffolds' mechanical performance, the three samples showed similar stress-strain curves. All samples were sterilized using gamma radiation, which can increase the crosslinking degree of PVA-based hydrogels. However, both irradiated samples, (SC)R and (3TSC)R, performed similarly to the non-irradiated SC samples.

In theory, additional crosslinking should increase hydrogel stiffness, but gamma radiation also produces free radicals that cause chain scission, weakening the material [80]. One study reported that gamma-irradiated chitosan showed neither crosslinking nor formation of new bonds, as confirmed by FTIR, indicating that random scission was the dominant reaction [81]. Another study showed that gamma radiation caused cellulose nanofibers to lose molecular weight and fiber length [82]. Overall, natural components in hydrogels tend to be weakened by irradiation.

Other factors may explain the lack of mechanical improvement after irradiation. The applied dose (29 kGy) is standard for sterilization but is not high enough to produce substantial reinforcement. A study found that low-dose irradiation (15 kGy) increased polymer scaffold strength, whereas higher doses (50 kGy) decreased it [83]. By analogy, the dose used in this investigation may have exceeded the beneficial threshold, promoting degradation rather than strengthening.

In addition, HAp may have reduced crosslinking efficiency. Inorganic fillers can stabilize polymers by adsorbing free radicals and delaying oxidation [84]. HAp also suppresses radiolysis [85], supporting its radical-scavenging capacity. Thus, although some beneficial crosslinking may have occurred, it was counterbalanced by PVA chain

scission, degradation of natural components and radical scavenging by HAp. These combined effects explain similar stress-strain curves and tangent modulus values.

Turning to the upper layer, the PVA hydrogels also produced an unexpected trend. In the non-irradiated 0T, 1T and 3T samples, mechanical strength increased with higher TA concentration, as expected (**Figure 17c, d**). In contrast, the irradiated samples showed the opposite behaviour: the irradiated pure PVA (0T) outer performed both 1T and 3T.

Tannic acid is a polyphenol rich in hydroxyl groups and forms strong hydrogen-bond crosslinks with PVA [57]. This explains the improved strength of non-irradiated samples with higher TA. However, TA also scavenges free radicals produced during gamma sterilization (like HAp) and is itself degraded by irradiation. As a result, irradiation prevents the formation of beneficial TA-PVA crosslinks and shifts the balance towards chain scission and material weakening [55, 60].

The FTIR results provide essential insight into the mechanical behaviour observed in the tangent compressive modulus tests by clarifying how gamma irradiation affected the chemical structure of the scaffolds. As shown in the FTIR spectra (**Figures 18–21**), the irradiated samples exhibited a noticeable broadening of the O–H stretching region and a smoothing of the amide and aromatic bands, indicating a reorganization of hydrogen bonding and partial degradation of chitosan and TA related structures. Additionally, the reduction in intensity of the PVA crystallinity band (around 1140–1080 cm^{-1}) reflects a loss of chain packing and possible chain scission. These molecular alterations generate two opposing mechanical effects: while increased intermolecular interactions can stiffen the network, decreased crystallinity and polymer degradation tend to reduce stiffness. In composite samples such as SC and 3TSC, the presence of chitosan, CNFs, HAp, and TA (confirmed through characteristic peaks in **Figures 18–19**) introduces physical reinforcement but also contributes to radical scavenging, which limits the extent of irradiation-induced crosslinking. As a result, the competing effects of limited crosslinking and polymer degradation are consistent with the modest differences observed in the tangent compressive modulus values (**Figure 23**), rather than a substantial increase in stiffness following irradiation.

As the bi-layer scaffolds attempt to replicate both the mechanical support of subchondral regions and the lubricious superficial zone, it becomes essential to compare

their compressive and tribological properties with those of native cartilage as well as with similar engineered materials reported in the literature. A study focused on a PVA/chitosan-based scaffold, reinforced with nano silica dioxide displayed values in wet conditions with a compressive strength of ~ 0.24 MPa. This study shows that the results for compressive strength in wet conditions greatly reduce the sample's stiffness, while with dry conditions results approach ~ 8.5 MPa [86]. A different study explores a similar based hydrogel (PVA/chitosan) but with the addition of HAp into the mixture. Compressive results exhibited in dry conditions a compressive strength of ~ 9.3 MPa [87]. This could indicate that the presence of HAp in the hydrogel could improve its mechanical performance. Despite the difference in compressive strength being spotted on dry conditions, it possible to assume that the same behaviour could be applied to the wet samples, explaining the slightly higher compressive modulus of the samples developed in the present study (0.5MPa – 1.5MPa, on a 5% to 20% strain range).

A comparison was conducted with studies that developed products like the one synthesized in this study for the same application. A key takeaway from literature is that very few studies focus on products comparable to the present paper. Most previously developed materials are primarily hydrogels rather than polymeric scaffolds for cartilage tissue engineering. A study investigating PVA-Based scaffolds for cartilage tissue engineering reported a maximum compressive modulus across all developed variations of ~ 0.2 MPa [88]. Similarly, another study reported that semi-degradable scaffolds seeded with cells achieved a compressive modulus of ~0.25 MPa [89]. When comparing the results obtained in the current study, in which the tangent compressive modulus of the (3TSC)R samples range from ~ 0.5 MPa to ~ 1.5 MPa, it is evident that the mechanical performance of the bi-layer scaffold developed is orders of magnitude higher than the values reported in the literature.

Native articular cartilage is significantly stiffer than most soft hydrogels. In slow unconfined compression tests, human femoral condyle cartilage shows a compressive modulus on the order of 5-13 MPa, (mean ~10.6 MPa at low strain), measured from ~0-20% strain [14]. This is much higher than the wet moduli of typical PVA/CS scaffolds (often <1 MPa). In contrast, under rapid loading cartilage exhibits a much higher instantaneous stiffness (~50MPa) [14].

In vivo, human knee cartilage deforms only modestly under normal activities. A study found that standing induces about -5.1% axial strain in tibiofemoral cartilage, which is largely recovered by walking [90]. This implies everyday cartilage strains of only a few percent. By testing the developed scaffolds to 20% strain, the study exceeds the normal cartilage deformations. It is therefore meaningful to compare tangent moduli at small strains; cartilage ~5-10% correspond to the linear regime. In that regime, cartilage's tangent modulus (~10 MPa) is higher that the developed scaffold. The bi-layer scaffold's tangent modulus (from 5-20% curves) should ideally approach cartilage's modulus to mimic load support, but complete equivalence is often hard to achieve.

In the tribological tests of the PVA/TA upper layer, all samples showed similar steady-state friction. However, the 0T samples exhibited an increasing CoF, while 1T and 3T showed decreasing trends. The rise in CoF for 0T can be attributed to fluid support: initially, interstitial water supports load and limits deformation, but as water is expelled, friction increases [91]. Gamma irradiation further contributes by reducing water retention in the 0T samples due to additional crosslinks [78].

In contrast, the 1T and 3T samples benefit from the gradual formation of a boundary film, enhanced by protein adsorption, from the synovial fluid analogue, which lowers friction over time [76]. Furthermore, although TA scavenges radicals, irradiation can still induce some sacrificial bonds between PVA and TA, reducing crystallinity and maintaining flexibility and water retention [92]. These combined mechanisms explain the mechanical and tribological behaviours observed.

PVA hydrogels alone are known to have a relatively high friction, but doping with tannic acid greatly reduces it. A study reported that just a 0.5 wt% addition of TA to a PVA hydrogel could lower its CoF to ~0.045 in PBS, which is about 2,7 times lower than a pure PVA hydrogel under identical conditions [76]. By comparison, pure PVA hydrogels have reported CoFs on the order of ~ 0.08-0.18 [93]. Thus, the developed upper PVA/TA layer, which exhibited values ~ 0.09 is aligned with the known values for pure PVA, despite a small improvement being noticed from the comparison of the pure PVA samples versus the TA doped samples.

To contextualize the performance of the developed bi-layer scaffold, it is essential to compare its mechanical and tribological behaviour to that of native articular cartilage,

whose unique combination of load-bearing capacity and ultralow friction sets the physiological benchmark for joint function.

Articular cartilage is extraordinarily well lubricated. Measured friction coefficients for cartilage-on-cartilage in synovial joints are extremely low, on the order of 0.001 to 0.03 [94]. In fact, cartilage under physiological pressure (~1 MPa) has CoF ~0.001 [94]. By comparison, even the best PVA/TA hydrogels have CoFs (~0.04 – 0.05) an order of magnitude higher. In other words, native cartilage friction is ~10-100 times lower than that of a PVA-based hydrogel [94]. The bi-layer scaffold's upper surface (PVA/TA) aims to reduce friction, but it is still well above the range of healthy cartilage (~0.001-0.03).

In summary, the bi-layer scaffold presents mechanical and tribological characteristics that align with the expected behaviour of PVA-based hydrogels modified with chitosan, HAp, and TA. Its compressive response and frictional performance fall within the ranges reported for similar engineered materials, particularly under hydrated conditions. When compared with native articular cartilage, differences remain in both stiffness and lubrication efficiency, reflecting the distinct structural and biomechanical composition of biological tissue. However, when compared with similar structures (scaffolds), it is evident that the developed composite structures carry a significant improvement in mechanical performance.

6. Conclusion

This dissertation presented the development of a composite bi-layer hydrogel-scaffold construct designed for articular cartilage regeneration, addressing the persistent clinical challenge of re-establishing the mechanical robustness, lubrication, and biological integration of damaged cartilage. The proposed system, referred to as the 3TSC construct, consists of a lower robocasted scaffold (PVA, hydroxyapatite, chitosan, and cellulose nanofibers) engineered to provide mechanical support and promote cell adhesion, and an upper cast-dried PVA/tannic acid hydrogel layer tuned to reduce friction and enhance surface adhesion. During the drying phase, the upper layer infiltrates the scaffold, forming a single integrated bi-layer architecture.

The system was fabricated via additive manufacturing for the scaffold and cast-drying for the hydrogel layer, followed by sterilization through gamma irradiation. One of the key achievements of this study was demonstrating that the composite material could be printed using robocasting with precision, consistency, and repeatability, confirming its suitability for additive manufacturing of reproducible, patient-specific scaffolds. Extensive morphological, mechanical, tribological, and biological evaluations confirmed that the scaffold and hydrogel layers perform their intended functions and integrate effectively. Morphological characterization showed adequate porosity in the scaffold and a smooth hydrogel surface, while tribological tests demonstrated improved lubrication. Biocompatibility assays confirmed high cell viability and adhesion, particularly in non-sorbitol formulations, supporting the scaffold's potential as a safe and functional substrate for cartilage regeneration.

Mechanical testing demonstrated that the (3TSC)R samples exhibited performance superior to similar scaffolds reported in the literature, with tannic acid contributing to improved lubrication under physiological conditions. Chemical analysis revealed the successful incorporation of all components, while also highlighting the influence of gamma irradiation. Although irradiation ensured sterilization, it affected the material's structure, potentially through bond cleavage in the scaffold polymers or degradation of

natural components, and its retention by hydroxyapatite and tannic acid likely reduced hydrogel crosslinking, influencing swelling and mechanical behaviour.

Overall, the bi-layer construct demonstrates a strong potential as a regenerative approach for cartilage repair, combining mechanical stability, low friction, and excellent biocompatibility. Future work should focus on refining irradiation conditions, improving long-term adhesion in wet environments, and conducting extended mechanical and tribological testing under physiological loading. Even so, the results represent a meaningful contribution to cartilage tissue engineering and highlight the relevance of combining engineered biomaterials with additive manufacturing technologies.

Bibliography

[1] V. Ulici, A. F. Chen, A. W. M. Cheng, and R. S. Tuan, “Anatomy, Cartilage,” *Hip Joint Restoration*, pp. 15–22, Oct. 2022, doi: 10.1007/978-1-4614-0694-5_2.

[2] T. Oláh, T. Kamarul, H. Madry, and M. R. Murali, “The Illustrative Anatomy and the Histology of the Healthy Hyaline Cartilage,” *The Illustrative Book of Cartilage Repair*, pp. 5–10, Jan. 2021, doi: 10.1007/978-3-030-47154-5_2.

[3] S. Posniak, J. H. Y. Chung, X. Liu, P. Mukherjee, and G. G. Wallace, “The importance of elastin and its role in auricular cartilage tissue engineering,” *Bioprinting*, vol. 32, p. e00276, Jul. 2023, doi: 10.1016/J.BPRINT.2023.E00276.

[4] J. L. Buchanan, “Types of Fibrocartilage,” *Clin Podiatr Med Surg*, vol. 39, no. 3, pp. 357–361, Jul. 2022, doi: 10.1016/J.CPM.2022.02.001.

[5] J. Eschweiler *et al.*, “The Biomechanics of Cartilage—An Overview,” *Life 2021, Vol. 11, Page 302*, vol. 11, no. 4, p. 302, Apr. 2021, doi: 10.3390/LIFE11040302.

[6] Y. Yu, J. Wang, Y. Li, Y. Chen, and W. Cui, “Cartilaginous Organoids: Advances, Applications, and Perspectives,” *Adv Nanobiomed Res*, vol. 3, no. 1, p. 2200114, Jan. 2023, doi: 10.1002/ANBR.202200114.

[7] M. Mostakhdemin, A. Nand, and M. Ramezani, “Articular and Artificial Cartilage, Characteristics, Properties and Testing Approaches—A Review,” *Polymers 2021, Vol. 13, Page 2000*, vol. 13, no. 12, p. 2000, Jun. 2021, doi: 10.3390/POLYM13122000.

[8] D. D. Chan, L. Cai, K. D. Butz, S. B. Trippel, E. A. Nauman, and C. P. Neu, “In vivo articular cartilage deformation: noninvasive quantification of intratissue strain during joint contact in the human knee,” *Scientific Reports 2016 6:1*, vol. 6, no. 1, pp. 1–14, Jan. 2016, doi: 10.1038/srep19220.

[9] C. J. Little, N. K. Bawolin, and X. Chen, “Mechanical Properties of Natural Cartilage and Tissue-Engineered Constructs,” *https://home.liebertpub.com/teb*, vol. 17, no. 4, pp. 213–227, Apr. 2011, doi: 10.1089/TEN.TEB.2010.0572.

[10] M. Tamaddon, L. Wang, Z. Liu, and C. Liu, “Osteochondral tissue repair in osteoarthritic joints: clinical challenges and opportunities in tissue engineering,” *Bio-Design and Manufacturing 2018 1:2*, vol. 1, no. 2, pp. 101–114, May 2018, doi: 10.1007/S42242-018-0015-0.

[11] C. J. Little, N. K. Bawolin, and X. Chen, “Mechanical Properties of Natural Cartilage and Tissue-Engineered Constructs,” *https://home.liebertpub.com/teb*, vol. 17, no. 4, pp. 213–227, Apr. 2011, doi: 10.1089/TEN.TEB.2010.0572.

[12] P. Krakowski, A. Rejniak, J. Sobczyk, and R. Karpiński, “Cartilage Integrity: A Review of Mechanical and Frictional Properties and Repair Approaches in Osteoarthritis,” *Healthcare*, vol. 12, no. 16, p. 1648, Aug. 2024, doi: 10.3390/HEALTHCARE12161648.

[13] D. Warnecke *et al.*, “Articular cartilage and meniscus reveal higher friction in swing phase than in stance phase under dynamic gait conditions,” *Scientific Reports 2019 9:1*, vol. 9, no. 1, pp. 5785-, Apr. 2019, doi: 10.1038/s41598-019-42254-2.

[14] W. Kabir, C. Di Bella, P. F. M. Choong, and C. D. O’Connell, “Assessment of Native Human Articular Cartilage: A Biomechanical Protocol,” *Cartilage*, vol. 13, no. 2_suppl, pp. 427S-437S, Dec. 2021, doi: 10.1177/1947603520973240;JOURNAL:JOURNAL:CARA;PAGE:STRING:ARTICLE/CHAPTER.

[15] F. Abreu dos Santos, A. Paula Valagão Amadeu do Serro Célio Gabriel Figueiredo Pina, J. Manuel Ferreira Morgado Supervisor, and C. Gabriel Figueiredo Pina, “Nomex ® Reinforced Poly (Vinyl Alcohol)-based Hydrogels for Articular Cartilage Replacement Bioengineering and Nanossystems Examination Committee,” 2022.

[16] R. Karpiński *et al.*, “Articular Cartilage: Structure, Biomechanics, and the Potential of Conventional and Advanced Diagnostics,” *Applied Sciences 2025, Vol. 15, Page 6896*, vol. 15, no. 12, p. 6896, Jun. 2025, doi: 10.3390/APP15126896.

[17] M. E. Kupratis, A. E. Gure, K. F. Ortved, D. L. Burris, and C. Price, “Comparative Tribology: Articulation-induced Rehydration of Cartilage Across Species,” *Biotribology*, vol. 25, p. 100159, Mar. 2021, doi: 10.1016/J.BIOTRI.2020.100159.

[18] X. Zhang, Y. Hu, K. Chen, and D. Zhang, “Bio-tribological behavior of articular cartilage based on biological morphology,” *Journal of Materials Science: Materials in Medicine 2021 32:11*, vol. 32, no. 11, pp. 132-, Oct. 2021, doi: 10.1007/S10856-021-06566-Y.

[19] K. D. Allen, L. M. Thoma, and Y. M. Golightly, “Epidemiology of osteoarthritis,” *Osteoarthritis Cartilage*, vol. 30, no. 2, pp. 184–195, Feb. 2022, doi: 10.1016/J.JOCA.2021.04.020.

[20] “Osteoarthritis.” Accessed: Nov. 16, 2025. [Online]. Available: https://www.who.int/news-room/fact-sheets/detail/osteoarthritis

[21] A. F. Radu and S. G. Bungau, “Management of Rheumatoid Arthritis: An Overview,” *Cells 2021, Vol. 10, Page 2857*, vol. 10, no. 11, p. 2857, Oct. 2021, doi: 10.3390/CELLS10112857.

[22] “Rheumatoid arthritis.” Accessed: Nov. 16, 2025. [Online]. Available: https://www.who.int/news-room/fact-sheets/detail/rheumatoid-arthritis

[23] R. P. Blom, D. Rahim, E. Paardekam, G. M. M. J. Kerkhoffs, D. Iannuzzi, and T. H. Smit, “A Traumatic Impact Immediately Changes the Mechanical Properties of Articular Cartilage,” *Cartilage*, Oct. 2024, doi: 10.1177/19476035241235633;REQUESTEDJOURNAL:JOURNAL:CARA;WGROUP:STRING:PUBLICATION.

[24] D. D. Anderson *et al.*, “Post-traumatic osteoarthritis: Improved understanding and opportunities for early intervention,” *Journal of Orthopaedic Research*, vol. 29, no. 6, pp. 802–809, Jun. 2011, doi: 10.1002/JOR.21359;PAGEGROUP:STRING:PUBLICATION.

[25] K. Solanki, S. Shanmugasundaram, N. Shetty, and S. J. Kim, “Articular cartilage repair & joint preservation: A review of the current status of biological approach,” *J Clin Orthop Trauma*, vol. 22, p. 101602, Nov. 2021, doi: 10.1016/J.JCOT.2021.101602.

[26] J. Jarecki *et al.*, “Knee Cartilage Lesion Management—Current Trends in Clinical Practice,” *Journal of Clinical Medicine 2023, Vol. 12, Page 6434*, vol. 12, no. 20, p. 6434, Oct. 2023, doi: 10.3390/JCM12206434.

[27] H. Chen *et al.*, “Drilling and microfracture lead to different bone structure and necrosis during bone-marrow stimulation for cartilage repair,” *Journal of Orthopaedic Research*, vol. 27, no. 11, pp. 1432–1438, Nov. 2009, doi: 10.1002/JOR.20905;SUBPAGE:STRING:ABSTRACT;WEBSITE:WEBSITE:PERICLES;REQUESTEDJOURNAL:JOURNAL:1554527X;WGROUP:STRING:PUBLICATION.

[28] P. Zedde *et al.*, “Subchondral bone remodeling: comparing nanofracture with microfracture. An ovine in vivo study,” *Joints*, vol. 04, no. 02, pp. 087–093, 2016, doi: 10.11138/JTS/2016.4.2.087.

[29] M. S. Shive *et al.*, “BST-CarGel® Treatment Maintains Cartilage Repair Superiority over Microfracture at 5 Years in a Multicenter Randomized Controlled Trial,” *Cartilage*, vol. 6, no. 2, pp. 62–72, Apr. 2015, doi: 10.1177/1947603514562064;ISSUE:ISSUE:DOI.

[30] G. Bentley *et al.*, “A prospective, randomised comparison of autologous chondrocyte implantation versus mosaicplasty for osteochondral defects in the knee,” *Journal of Bone and Joint Surgery - Series B*, vol. 85, no. 2, pp. 223–230, Mar. 2003, doi: 10.1302/0301-620X.85B2.13543/LETTERTOEDITOR.

[31] F. Hashemi-Afzal, H. Fallahi, F. Bagheri, M. N. Collins, M. B. Eslaminejad, and H. Seitz, “Advancements in hydrogel design for articular cartilage regeneration: A comprehensive review,” *Bioact Mater*, vol. 43, pp. 1–31, Jan. 2025, doi: 10.1016/J.BIOACTMAT.2024.09.005.

[32] S. Bashir *et al.*, “Fundamental Concepts of Hydrogels: Synthesis, Properties, and Their Applications,” *Polymers (Basel)*, vol. 12, no. 11, p. 2702, Nov. 2020, doi: 10.3390/POLYM12112702.

[33] U. S. K. Madduma-Bandarage and S. V. Madihally, “Synthetic hydrogels: Synthesis, novel trends, and applications,” *J Appl Polym Sci*, vol. 138, no. 19, May 2021, doi: 10.1002/APP.50376.

[34] “20. Chemical structure of poly(vinyl-alcohol) (PVA) [cf. Chapter 1,... | Download Scientific Diagram.” Accessed: Nov. 28, 2025. [Online]. Available: https://www.researchgate.net/figure/Chemical-structure-of-polyvinyl-alcohol-PVA-cf-Chapter-1-Insulators_fig19_272168061

[35] A. Romero García and M. Bercea, “Recent Advances in Poly(vinyl alcohol)-Based Hydrogels,” *Polymers 2024, Vol. 16, Page 2021*, vol. 16, no. 14, p. 2021, Jul. 2024, doi: 10.3390/POLYM16142021.

[36] C. Luo, A. Guo, Y. Zhao, and X. Sun, “A high strength, low friction, and biocompatible hydrogel from PVA, chitosan and sodium alginate for articular cartilage,” *Carbohydr Polym*, vol. 286, p. 119268, Jun. 2022, doi: 10.1016/J.CARBPOL.2022.119268.

[37] “Chemical structure of chitosan. | Download Scientific Diagram.” Accessed: Nov. 28, 2025. [Online]. Available: https://www.researchgate.net/figure/Chemical-structure-of-chitosan_fig4_355787682

[38] Y. Chen, M. Yang, W. Zhang, W. Guo, X. Zhang, and B. Zhang, “Facile Preparation of Irradiated Poly(vinyl alcohol)/Cellulose Nanofiber Hydrogels with Ultrahigh Mechanical Properties for Artificial Joint Cartilage,” *Materials 2024, Vol. 17, Page 4125*, vol. 17, no. 16, p. 4125, Aug. 2024, doi: 10.3390/MA17164125.

[39] “Chemical structure of cellulose. | Download Scientific Diagram.” Accessed: Nov. 28, 2025. [Online]. Available: https://www.researchgate.net/figure/Chemical-structure-of-cellulose_fig1_282808433

[40] M. B. Jalageri *et al.*, “Hydroxyapatite Reinforced Polyvinyl Alcohol/Polyvinyl Pyrrolidone Based Hydrogel for Cartilage Replacement,” *Gels 2022, Vol. 8, Page 555*, vol. 8, no. 9, p. 555, Sep. 2022, doi: 10.3390/GELS8090555.

[41] “Chemical structure of hydroxyapatite, Ca 10 (PO 4) 6 (OH) 2 | Download Scientific Diagram.” Accessed: Nov. 28, 2025. [Online]. Available: https://www.researchgate.net/figure/Chemical-structure-of-hydroxyapatite-Ca-10-PO-4-6-OH-2_fig8_47933950

[42] H. Li, J. Li, T. Li, C. Wu, and W. Zhang, “Macroporous polyvinyl alcohol-tannic acid hydrogel with high strength and toughness for cartilage replacement,” *Journal of Materials Science 2022 57:17*, vol. 57, no. 17, pp. 8262–8275, Apr. 2022, doi: 10.1007/S10853-022-07209-5.

[43] “Chemical structure of Tannic acid | Download Scientific Diagram.” Accessed: Nov. 28, 2025. [Online]. Available: https://www.researchgate.net/figure/Chemical-structure-of-Tannic-acid_fig7_313638203

[44] T. A. Yeshiwas, A. B. Tiruneh, and M. A. Sisay, “A review article on the assessment of additive manufacturing,” *Journal of Materials Science: Materials in Engineering 2025 20:1*, vol. 20, no. 1, pp. 85-, Jul. 2025, doi: 10.1186/S40712-025-00306-8.

[45] S. Lamnini, H. Elsayed, Y. Lakhdar, F. Baino, F. Smeacetto, and E. Bernardo, “Robocasting of advanced ceramics: ink optimization and protocol to

predict the printing parameters - A review," *Heliyon*, vol. 8, no. 9, p. e10651, Sep. 2022, doi: 10.1016/j.heliyon.2022.e10651.

[46] N. Johari, Z. Adabavazeh, and F. Baino, "PVA-based bioinks for 3D bioprinting: A comprehensive review of their applications in tissue engineering," *Bioprinting*, vol. 49, p. e00419, Sep. 2025, doi: 10.1016/J.BPRINT.2025.E00419.

[47] T. Wang, J. H. Lai, and F. Yang, "Effects of Hydrogel Stiffness and Extracellular Compositions on Modulating Cartilage Regeneration by Mixed Populations of Stem Cells and Chondrocytes In Vivo," *Tissue Eng Part A*, vol. 22, no. 23–24, p. 1348, Dec. 2016, doi: 10.1089/TEN.TEA.2016.0306.

[48] T. Luo, B. Tan, L. Zhu, Y. Wang, and J. Liao, "A Review on the Design of Hydrogels With Different Stiffness and Their Effects on Tissue Repair," *Front Bioeng Biotechnol*, vol. 10, p. 817391, Jan. 2022, doi: 10.3389/FBIOE.2022.817391/FULL.

[49] G. Bovone, O. Y. Dudaryeva, B. Marco-Dufort, and M. W. Tibbitt, "Engineering Hydrogel Adhesion for Biomedical Applications via Chemical Design of the Junction," Sep. 13, 2021, *American Chemical Society*. doi: 10.1021/acsbiomaterials.0c01677.

[50] G. D. Degen *et al.*, "Mussel-inspired cross-linking mechanisms enhance gelation and adhesion of multifunctional mucin-derived hydrogels," *Proc Natl Acad Sci U S A*, vol. 122, no. 8, p. e2415927122, Feb. 2025, doi: 10.1073/PNAS.2415927122;PAGE:STRING:ARTICLE/CHAPTER.

[51] W. Dou, X. Zeng, S. Zhu, Y. Zhu, H. Liu, and S. Li, "Mussel-Inspired Injectable Adhesive Hydrogels for Biomedical Applications," *International Journal of Molecular Sciences 2024, Vol. 25, Page 9100*, vol. 25, no. 16, p. 9100, Aug. 2024, doi: 10.3390/IJMS25169100.

[52] M. Suneetha, K. M. Rao, and S. S. Han, "Mussel-Inspired Cell/Tissue-Adhesive, Hemostatic Hydrogels for Tissue Engineering Applications," *ACS Omega*, vol. 4, no. 7, pp. 12647–12656, Jul. 2019, doi: 10.1021/ACSOMEGA.9B01302.

[53] Y. Meng *et al.*, "A review of advances in tribology in 2020–2021," *Friction 2022 10:10*, vol. 10, no. 10, pp. 1443–1595, Oct. 2022, doi: 10.1007/S40544-022-0685-7.

[54] D. M. Russell and D. T. Apatoczky, "Walking at the preferred stride frequency minimizes muscle activity," *Gait Posture*, vol. 45, pp. 181–186, Mar. 2016, doi: 10.1016/j.gaitpost.2016.01.027.

[55] "ISO 10993-12:2021 - Biological evaluation of medical devices — Part 12: Sample preparation and reference materials." Accessed: Nov. 16, 2025. [Online]. Available: https://www.iso.org/standard/75769.html

[56] H. S. Mansur, C. M. Sadahira, A. N. Souza, and A. A. P. Mansur, "FTIR spectroscopy characterization of poly (vinyl alcohol) hydrogel with different hydrolysis degree and chemically crosslinked with glutaraldehyde," *Materials*

Science and Engineering: C, vol. 28, no. 4, pp. 539–548, May 2008, doi: 10.1016/J.MSEC.2007.10.088.

[57] C. Si *et al.*, "A Polyvinyl Alcohol–Tannic Acid Gel with Exceptional Mechanical Properties and Ultraviolet Resistance," *Gels*, vol. 8, no. 11, p. 751, Nov. 2022, doi: 10.3390/GELS8110751.

[58] H. Kim, P. K. Panda, K. Sadeghi, and J. Seo, "Poly (vinyl alcohol)/hydrothermally treated tannic acid composite films as sustainable antioxidant and barrier packaging materials," *Prog Org Coat*, vol. 174, p. 107305, Jan. 2023, doi: 10.1016/J.PORGCOAT.2022.107305.

[59] J. Cheng *et al.*, "The physicochemical properties of chitosan prepared by microwave heating," *Food Sci Nutr*, vol. 8, no. 4, pp. 1987–1994, Apr. 2020, doi: 10.1002/FSN3.1486;WGROUP:STRING:PUBLICATION.

[60] I. Kouadri and H. Satha, "Extraction and characterization of cellulose and cellulose nanofibers from Citrullus colocynthis seeds," *Ind Crops Prod*, vol. 124, pp. 787–796, Nov. 2018, doi: 10.1016/J.INDCROP.2018.08.051.

[61] F. Gharbi *et al.*, "Structural, Thermal, and Optical Studies of Gamma Irradiated Polyvinyl Alcohol-, Lignosulfonate-, and Palladium Nanocomposite Film," *Polymers 2022, Vol. 14, Page 2613*, vol. 14, no. 13, p. 2613, Jun. 2022, doi: 10.3390/POLYM14132613.

[62] H. W. Park, N. G. Jang, H. S. Seo, K. Kwon, and S. Shin, "Facile Synthesis of Self-Adhesion and Ion-Conducting 2-Acrylamido-2-Methylpropane Sulfonic Acid/Tannic Acid Hydrogels Using Electron Beam Irradiation," *Polymers 2023, Vol. 15, Page 3836*, vol. 15, no. 18, p. 3836, Sep. 2023, doi: 10.3390/POLYM15183836.

[63] X. Liang *et al.*, "Polyvinyl Alcohol (PVA)-Based Hydrogels: Recent Progress in Fabrication, Properties, and Multifunctional Applications," *Polymers 2024, Vol. 16, Page 2755*, vol. 16, no. 19, p. 2755, Sep. 2024, doi: 10.3390/POLYM16192755.

[64] K. J. Gooch and C. J. Tennant, "Chondrocytes," *Mechanical Forces: Their Effects on Cells and Tissues*, pp. 79–100, 1997, doi: 10.1007/978-3-662-03420-0_4.

[65] M. M. Rahman Khan and M. M. H. Rumon, "Synthesis of PVA-Based Hydrogels for Biomedical Applications: Recent Trends and Advances," *Gels*, vol. 11, no. 2, p. 88, Feb. 2025, doi: 10.3390/GELS11020088.

[66] S. Mondal *et al.*, "Hydroxyapatite: A journey from biomaterials to advanced functional materials," *Adv Colloid Interface Sci*, vol. 321, p. 103013, Nov. 2023, doi: 10.1016/J.CIS.2023.103013.

[67] M. Mahardika *et al.*, "Nanocellulose reinforced polyvinyl alcohol-based bio-nanocomposite films: improved mechanical, UV-light barrier, and thermal properties," *RSC Adv*, vol. 14, no. 32, p. 23232, Jul. 2024, doi: 10.1039/D4RA04205K.

[68] X. Huang, Y. Wang, Y. Wang, and L. Yang, “A Facile One-Pot Preparation and Properties of Nanocellulose-Reinforced Ionic Conductive Hydrogels,” *Molecules*, vol. 28, no. 3, p. 1301, Feb. 2023, doi: 10.3390/MOLECULES28031301.

[69] S. R. Torab, M. M. Shehata, H. H. Saleh, and Z. I. Ali, “Physico-chemical properties of irradiated poly (vinyl alcohol)–Ethylene glycol blend films by γ-rays and ion beam,” *Polymers and Polymer Composites*, vol. 30, Jan. 2022, doi: 10.1177/09673911211063246;WGROUP:STRING:PUBLICATION.

[70] P. Li, C. Xiong, and W. Huang, “Gamma-Irradiation-Induced Degradation of the Water-Soluble Polysaccharide from Auricularia polytricha and Its Anti-Hypercholesterolemic Activity,” *Molecules 2022, Vol. 27, Page 1110*, vol. 27, no. 3, p. 1110, Feb. 2022, doi: 10.3390/MOLECULES27031110.

[71] O. Novotný, K. Cejpek, and J. Velíšek, “Formation of carboxylic acids during degradation of monosaccharides,” *Czech Journal of Food Sciences*, vol. 26, no. 2, pp. 117–131, 2008, doi: 10.17221/2465-CJFS.

[72] S. Malaiappan and J. Harris, “Osteogenic Potential of Magnesium Oxide Nanoparticles in Bone Regeneration: A Systematic Review,” *Cureus*, vol. 16, no. 3, p. e55502, Mar. 2024, doi: 10.7759/CUREUS.55502.

[73] B. A. Abdul-Majeed, H. K. Hussain, and N. A. K. Al-Sultanee, “Effect of Annealing on the Crystallization of Poly Vinyl Chloride for Drug Delivery System,” *Iraqi Journal of Chemical and Petroleum Engineering*, vol. 13, no. 2, pp. 29–36, Jun. 2012, doi: 10.31699/IJCPE.2012.2.3.

[74] Y. Liu *et al.*, “A mussel inspired polyvinyl alcohol/collagen/tannic acid bioadhesive for wet adhesion and hemostasis,” *Colloids Surf B Biointerfaces*, vol. 235, Mar. 2024, doi: 10.1016/j.colsurfb.2024.113766.

[75] X. Yu, J. Huang, C. Wu, and W. Zhang, “Biocompatible autonomous self-healing PVA-CS/TA hydrogels based on hydrogen bonding and electrostatic interaction,” *Scientific Reports 2025 15:1*, vol. 15, no. 1, pp. 1893-, Jan. 2025, doi: 10.1038/s41598-025-85298-3.

[76] Q. Li, Y. L. Gong, Y. Li, S. Li, W. L. Liang, and Y. X. Leng, “Study on the lubrication behavior of tannic acid/ poly (vinyl alcohol) hydrogel enhanced by protein adsorption for articular cartilage applications,” *J Mech Behav Biomed Mater*, vol. 162, p. 106825, Feb. 2025, doi: 10.1016/J.JMBBM.2024.106825.

[77] S. Barbon *et al.*, “Enhanced Biomechanical Properties of Polyvinyl Alcohol-Based Hybrid Scaffolds for Cartilage Tissue Engineering,” *Processes 2021, Vol. 9, Page 730*, vol. 9, no. 5, p. 730, Apr. 2021, doi: 10.3390/PR9050730.

[78] S. Sasaki, S. Omata, T. Murakami, N. Nagasawa, M. Taguchi, and A. Suzuki, “Effect of Gamma Ray Irradiation on Friction Property of Poly(vinyl alcohol) Cast-Drying on Freeze-Thawed Hybrid Gel,” *Gels 2018, Vol. 4, Page 30*, vol. 4, no. 2, p. 30, Mar. 2018, doi: 10.3390/GELS4020030.

[79] “From materials to clinical use: advances in 3D-printed scaffolds for cartilage tissue engineering - Physical Chemistry Chemical Physics (RSC

Publishing) DOI:10.1039/D3CP00921A." Accessed: Nov. 30, 2025. [Online]. Available: https://pubs.rsc.org/en/content/articlehtml/2023/cp/d3cp00921a

[80] A. T. Naikwadi, B. K. Sharma, K. D. Bhatt, and P. A. Mahanwar, "Gamma Radiation Processed Polymeric Materials for High Performance Applications: A Review," *Front Chem*, vol. 10, p. 837111, Mar. 2022, doi: 10.3389/FCHEM.2022.837111/BIBTEX.

[81] K. G. Desai and J. P. Hyun, "Study of gamma-irradiation effects on chitosan microparticles," *Drug Deliv*, vol. 13, no. 1, pp. 39–50, Jan. 2006, doi: 10.1080/10717540500309123.

[82] I. Ogura *et al.*, "Effect of gamma irradiation on cellulose nanofibers," *Journal of Wood Science 2025 71:1*, vol. 71, no. 1, pp. 37-, Jul. 2025, doi: 10.1186/S10086-025-02215-Y.

[83] J. X. Jiang, L. M. Li, L. L. Lin, Y. Zuo, Y. B. Li, and J. D. Li, "Effects of γ-Ray Irradiation on the Properties of Nano-Hydroxyapatite/Polyurethane Composite Porous Scaffolds," *Materials Science Forum*, vol. 852, pp. 422–427, 2016, doi: 10.4028/WWW.SCIENTIFIC.NET/MSF.852.422.

[84] T. Zaharescu, M. Râpa, I. Blanco, T. Borbath, and I. Borbath, "Durability of LDPE/UHMWPE Composites under Accelerated Degradation," *Polymers 2020, Vol. 12, Page 1241*, vol. 12, no. 6, p. 1241, May 2020, doi: 10.3390/POLYM12061241.

[85] J. R. Jokisaari, X. Hu, A. Mukherjee, V. Uskoković, and R. F. Klie, "Hydroxyapatite as a scavenger of reactive radiolysis species in graphene liquid cells for in situ electron microscopy," *Nanotechnology*, vol. 32, no. 48, Nov. 2021, doi: 10.1088/1361-6528/AC1EBB.

[86] W. Ma *et al.*, "Preparation of High Mechanical Strength Chitosan Nanofiber/NanoSiO2/PVA Composite Scaffolds for Bone Tissue Engineering Using Sol–Gel Method," *Polymers 2022, Vol. 14, Page 2083*, vol. 14, no. 10, p. 2083, May 2022, doi: 10.3390/POLYM14102083.

[87] A. Babakhani, S. J. Peighambardoust, and A. Olad, "Fabrication of magnetic nanocomposite scaffolds based on polyvinyl alcohol-chitosan containing hydroxyapatite and clay modified with graphene oxide: Evaluation of their properties for bone tissue engineering applications," *J Mech Behav Biomed Mater*, vol. 150, Feb. 2024, doi: 10.1016/j.jmbbm.2023.106263.

[88] H. D. Kim, Y. Lee, Y. Kim, Y. Hwang, and N. S. Hwang, "Biomimetically Reinforced Polyvinyl Alcohol-Based Hybrid Scaffolds for Cartilage Tissue Engineering," *Polymers 2017, Vol. 9, Page 655*, vol. 9, no. 12, p. 655, Nov. 2017, doi: 10.3390/POLYM9120655.

[89] Y. Cao, D. Xiong, Y. Niu, Y. Mei, Z. Yin, and J. Gui, "Compressive properties and creep resistance of a novel, porous, semidegradable poly(vinyl alcohol)/poly(lactic-co-glycolic acid) scaffold for articular cartilage repair," *J Appl Polym Sci*, vol. 131, no. 11, Jun. 2014, doi: 10.1002/APP.40311;WGROUP:STRING:PUBLICATION.

[90] S. J. Kust *et al.*, “Walking recovers cartilage compressive strain in vivo,” *Osteoarthr Cartil Open*, vol. 6, no. 4, Dec. 2024, doi: 10.1016/j.ocarto.2024.100526.

[91] Y. ; Feng *et al.*, “Tribological and Rheological Properties of Poly(vinyl alcohol)-Gellan Gum Composite Hydrogels,” *Polymers 2022, Vol. 14, Page 3830*, vol. 14, no. 18, p. 3830, Sep. 2022, doi: 10.3390/POLYM14183830.

[92] M. Yang, W. Guo, S. Liu, B. Zhang, Y. Chen, and Y. Wang, “Highly stretchable gamma-irradiated poly (vinyl alcohol)/Tannic acid composite hydrogels with superior transparency and antibacterial activity,” *Journal of Polymer Research 2021 28:11*, vol. 28, no. 11, pp. 412-, Oct. 2021, doi: 10.1007/S10965-021-02777-7.

[93] F. Li, Y. Su, J. Wang, G. Wu, and C. Wang, “Influence of dynamic load on friction behavior of human articular cartilage, stainless steel and polyvinyl alcohol hydrogel as artificial cartilage,” *J Mater Sci Mater Med*, vol. 21, no. 1, pp. 147–154, Jan. 2010, doi: 10.1007/S10856-009-3863-5.

[94] S. Jahn and J. Klein, “Lubrication of articular cartilage,” *Phys Today*, vol. 71, no. 4, pp. 48–54, Apr. 2018, doi: 10.1063/PT.3.3898.

Appendices

A. Sorbitol Samples Cell Viability

Table 5 - Cell viability of samples scaffold

%	S.SC (*)	S.SC (1:10)
1	13,80	61,85
2	21,86	62,66
3	17,73	68,47
4	22,39	78,31
5	19,90	58,80
Average	19,14	66,02

containing sorbitol. (*) Samples that included sorbitol are referred to as S.SC.